AMERICAN UNIVERSITY OF BEIRUT

ASSESSMENT OF LAI DERIVED FROM HARMONIZED LANDSAT SENTINEL-2 (HLS), S2 THEIA, AND SNAP FOR CROPS IN THE BEKAA, LEBANON

by
ROYA AHMAD MOURAD

A thesis
submitted in partial fulfillment of the requirements
for the degree of Master of Science
to the Department of Irrigation
of the Faculty of Agriculture and Food Science
at the American University of Beirut

Beirut, Lebanon
May 2020

AMERICAN UNIVERSITY OF BEIRUT

ASSESSMENT OF LAI DERIVED FROM HARMONIZED LANDSAT SENTINEL-2 (HLS), S2 THEIA, AND SNAP FOR CROPS IN THE BEKAA, LEBANON

by

ROYA AHMAD MOURAD

Approved by:

Dr. Hadi Jaafar, Assistant Professor — Advisor
Agriculture Sciences

Dr. Issmat Kassem, Assistant Professor — Member of Committee
Nutrition and Food Sciences

Dr. Ali Chalak, Associate Professor — Member of Committee
Agriculture Sciences

Date of thesis defense: May 4, 2020

AMERICAN UNIVERSITY OF BEIRUT

THESIS, DISSERTATION, PROJECT RELEASE FORM

Student Name:
___Mourad_____Roya_____Ahmad_____

Last First Middle

⊗ Master's Thesis ⬭ Master's Project ⬭ Doctoral Dissertation

☐ I authorize the American University of Beirut to: (a) reproduce hard or electronic copies of my thesis, dissertation, or project; (b) include such copies in the archives and digital repositories of the University, and (c) make freely available such copies to third parties for research or educational purposes.

☒ I authorize the American University of Beirut, to: (a) reproduce hard or electronic copies of it; (b) include such copies in the archives and digital repositories of the University; and (c) make freely available such copies to third parties for research or educational purposes

after:

One --☒-- year from the date of submission of my thesis, dissertation, or project.

Two ---- years from the date of submission of my thesis, dissertation, or project.

Three ---- years from the date of submission of my thesis, dissertation, or project.

__Roya Mourad_____

Signature Date: May 18, 2020

ACKNOWLEDGMENTS

I would like first to thank my advisor, Dr. Hadi Jaafar, for his constant support and motivation to present this research work. Without his guidance and mentorship, this thesis would not have been possible.

I would also like to thank my committee members, Dr. Issmat Kassem and Dr. Ali Chalak, for their guidance and remarks.

Very thankful to Mrs. Nadine Knesevitch at the Jafet Library Archives and Special Collections Department for helping me with the formatting of my thesis.

I would also wish to express my gratitude to my family, especially my mom and dad, for their endless love and support throughout my graduate studies. A big thanks, to my sister Aya, for her help and for always being by my side through this journey. Thanks a lot, to all my sisters and brothers, for their encouragement and supporting words.

To all my friends, thank you for all the moments we spent together through this process. Many thanks to Naji for helping me in conducting the field campaigns. All the love and gratitude to my friend Farah. Very thankful to Nour Ezzddine, Mohamad Ali, Nour El Korek, Lora, Hawraa, Walaa, Rachel, Gadson, Razan, and Imad, for making me feel at ease along the way.

This work was made possible through funds of NASA Grant 17-LCLUC17-0002“Characterizing Field-Scale Water Use, Phenology and Productivity in Agricultural Landscapes using Multi-Sensor Data Fusion,” through a subcontract from the USDA. Special thanks to Dr. Martha Anderson of the Hydrology and Remote Sensing Lab for her valuable comments.

AN ABSTRACT OF THE THESIS OF

Roya Ahmad Mourad for Master of Science
Major: Irrigation

Title: Assessment of LAI derived from HLS Landsat Sentinel-2, S2 THEIA, and SNAP for crops in Bekaa (Lebanon)

Background: Leaf area index (LAI) is an essential indicator of crop development and growth. Proper satellite-based LAI estimates at the farm-level often require near-daily imagery at medium to high spatial resolution. The combination of data from different ongoing satellite missions, Sentinel 2 (ESA) and Landsat 8 (NASA), provides this opportunity.

Objectives: In this study, we evaluated the leaf area index generated from three products, namely: the harmonized surface reflectance produced by NASA, SNAP biophysical model, and L2A THEIA's product from Sentinel-2 for the agricultural scheme in Bekaa (Lebanon).

Methods: For this purpose, we used a broad set of in-field LAI measurements collected in a wide variety of canopy structures during the 2018 and 2019 growing seasons. The dynamics of LAI and crop height were monitored during the 2019 growing season. We further assessed the validity of existing LAI models and evaluated the relationship between the studied vegetation indices and the ground measured LAI. Also, crop-specific height – LAI and above-ground biomass– LAI equations were generated.

Results: Results show when comparing the measured LAI to the LAI Models existing in Literature that LAI models, which were derived from EVI2 statistically performed better than other models for the combined crops. LAI derived from the artificial neural network through ESA's SNAP biophysical processor is underestimated. Additionally, the red-edge bands used in the S2 SeLI LAI algorithm offers an improved LAI crop biophysical parameter retrieval with low errors following the HLS LAI Models. Also, our findings show that the LAI-VIs relationship is crop-specific. Among the examined indices, EVI2 outperformed other indices for the crops combined (R2:0.6, RMSE: 1.00, and p-value <0.0001), thus, EVI2 derived from the HLS product can be identified as a best suited for a unified algorithm.

CONTENTS

ILLUSTRATIONS

Figure Page

TABLES

ABBREVIATIONS

AGDB	Above-ground dry biomass
ANN	Artificial Neural Network
HLS	Harmonized Landsat Sentinel-2 Product
LAI	Leaf Area Index
NDVI	Normalized Difference Vegetation Index
NIR	Near-Infrared Reflectance
RMSE	Root Mean Square Error
RTM	Radiative Transfer Model
RS	Remote sensing
SAVI	Soil Adjusted Vegetation Index
SNAP	Sentinel Application Platform
TM	Thematic Mapper
VIs	Vegetation Indices
LUE	Light Use Efficiency
NDVI	Normalized Difference Vegetation Index

CHAPTER I

INTRODUCTION

A. Background

One of the most fundamental vegetation biophysical parameters is the Leaf Area Index (LAI), defined as a dimensionless measure of the one-sided leaf area (m2) per unit ground surface area (m2) (Asner et al. 2003; Chen et al. 1992). LAI has long been reported as a good indicator for several agronomic, ecological, and hydrological applications such as vegetation status (Reyes-González et al. 2019), atmospheric circulation models (Charbonnier 2013), photosynthesis and biomass accumulation (Viña et al. 2011b), evapotranspiration (Jung et al. 2010), hydrological models (Jung et al. 2010), climate change (Fassnacht et al. 1997), and rainfall interception (Taugourdeau et al. 2014). LAI is also crucial in several land surface models (Jarlan et al. 2008; van den Hurk et al. 2003), crop yield models, and yield estimation (Dente et al. 2008; Fang et al. 2008).

There are two major divisions in terms of LAI measurement methods: (1) direct measurement and (2) indirect measurement. The direct method involves destructively harvesting the canopy and measuring the area of the collected leaves samples through instruments such as LI-3000C Portable Leaf Area Meter (LI-COR, Lincoln, NE, USA). This method has relatively high precision, and it is often used to validate the indirect measurement methods; however, it is very labor-intensive, tedious, and is not suitable for large area measurement (Breda 2003; Feng et al. 2019). On the other hand, the indirect methods are based on light interception, hemispherical photography, or remote

sensing (Ariza-Carricondo et al. 2019). Both light interception and hemispherical techniques are referred to as optical approaches, which involve variables measurements such as gap fraction and light transmission. These variables are measured by commercial instruments and are related to LAI based on PAR inversion and Beer-Lambert extinction law theories for both gap fraction and light transmission, respectively.

Several researchers used different optical instruments to either assess these instruments against direct measurements or to validate the remotely sensed LAI. Although the indirect measurement of LAI using optical instruments is faster than direct measurements, it suffers from several limitations. First, indirect measurements do not measure the LAI but rather the light intercepted by the plant canopy that is then related to LAI. In other words, the optical instruments do not distinguish the leaves from the flowers or branches. Thus, they tend to either underestimate or overestimate the direct LAI depending on the method used and canopy studied.

Moreover, each method has some sources of error. For example, the digital hemispherical photography (DHP) includes some subjectivity for factors such as variable clouds, shadows, and brightness, which makes it challenging to choose a threshold that allows distinguishing canopy from non-canopy. For this reason, the hemispherical photographs are recommended to be captured under uniformly diffuse or overcast conditions, while the leaf angle distribution can be a source of error if it is misestimated in instruments such as SS1 and AccuPAR. Finally, row spacing, crop height, time of measurement, and placement of the meter can affect the observed LAI values.

In this vein, remote sensing has proved to be a promising alternative tool for estimating crop LAI without damage, in a fast way, and with a large spatial variability (Hansen et al. 2003; He et al. 2016). Despite these advantages, remote sensing requires validation with ground truth data (Ariza-Carricondo et al. 2019). The retrieval of crop biophysical variables from remote sensing falls into two categories: the empirical and physical modeling approaches. The simplest yet the most effective method of estimating LAI from remote sensing is by establishing an empirical relationship between the remotely sensed vegetation indices (VIs) and measured LAI, referred to as the LAI-VI approach (Baret and Guyot 1991; Broge and Leblanc 2001). Vegetation indices are computed based on the reflectance of two or more bands, and it reflects the biophysical characteristics of the plant canopy such as greenness, biomass, and LAI (Baghzouz et al. 2010; Huete et al. 1996). VIs have shown to correlate well with LAI such as Normalized Difference Vegetation Index (NDVI) (Deering 1978), Soil Adjusted Vegetation Index (SAVI) (Huete 1988), Enhanced Vegetation Index (EVI) (Huete et al. 1997), and Enhanced Vegetation Index 2 (EVI2) (Jiang et al. 2008). This correlation takes various mathematical forms, such as linear, logarithmic, polynomial, or exponential (Nguy-Robertson et al. 2014; Viña et al. 2011b).

On the other hand, the physical modeling approach involves the use of the radiative transfer models (RTMs) to simulate the canopy spectral reflectance, and the inversion of RTMs to obtain the required parameters (Campos-Taberner et al. 2016; Féret et al. 2017). One of the physical modeling techniques is the retrieval of LAI biophysical parameter based on neural networks, such as the algorithm implemented Sentinel Application Platform (SNAP) biophysical processor tool (Weiss and Baret 2016), developed by the European Space Agency (ESA). However, the accuracy of the

LAI product using the SNAP software has been poorly assessed, generating primarily improvable results (Djamai and Fernandes 2018; Pasqualotto et al. 2019b). The LAI biophysical parameter retrieval of a wide range of crop varieties is yet to be evaluated with SNAP.

Despite the advances in technology allowing remote sensing to play a vital role in LAI estimate, the trade-off between the temporal and spatial resolution (Strittholt et al. 2007) has limited the ability of a single sensor to capture the crop LAI dynamics and its heterogeneity at the farm level. Several studies pointed out that medium spatial resolution products (e.g., Landsat 30 m spatial resolution) potentially miss the observations at critical growth stages due to their long revisit time (16 days) (Hansen and Loveland 2012; Hilker et al. 2009; Yang et al. 2015). Therefore, proper LAI monitoring, especially during fast-developing phenomena, requires daily or near-daily imagery at medium to high spatial resolution (10–30 m) (Claverie et al. 2012; Skakun et al. 2017). One of the techniques that aim to increase data resolution is the Spatio-temporal image fusion (or sensor fusion). This approach generates finer spatial resolution images via synthesizing the high spatial-low temporal products (e.g., Landsat), with the coarse spatial and the high temporal resolution of the products (e.g., MODIS) while maintaining the frequency (Boschetti et al. 2015; Ma et al. 2018; Wang et al. 2017). However, this approach involves considerable uncertainty (Wang et al. 2017) due to (1) the loss of the spectral signatures of small objects in the fused images (Behnia 2005), and (2) the low co-registration accuracy due to the significant difference in the sensors' resolution (Dong et al. 2009). The proven compatibility between Landsat 8 and Sentinel-2 bands enables the opportunity for LAI estimation at near-daily medium resolution by merging their observations (Barsi et al. 2018; Storey et al. 2016). In this

context, NASA has developed a new Harmonized Landsat and Sentinel-2 (HLS) product. HLS consists of surface reflectance (SR) data from the Operational Land Imager (OLI) and Multi-Spectral Instrument (MSI) onboard the Landsat 8 and Sentinel-2 remote sensing satellites, respectively. The advantage of the HLS product is that it can provide a near-real-time agriculture monitoring at a moderate spatial resolution (<30 m) (Claverie et al. 2018).

B. Problem Statement and Definition

1. Problem Statement

- Pre-existing LAI Models from the previous literature may only be applicable to the study areas, and land cover types to which the LAI Models have been applied
- Based on the above, these LAI models require validation with ground truth data
- Several researchers either rely solely on a daily but coarse resolution sensor or a long-term revisit time but high spatial resolution sensor, with a limitation of a single sensor to capture the LAI dynamics at critical crop growth stages.

2. Research questions

- Can the existing LAI models be applied to the study area?
- Moreover, how accurate are they?
- Can we produce new LAI models specific to our studied crops?

- Can we obtain near real-time LAI observations with medium to a high spatial resolution?

3. Research objectives

Therefore, the present work aims to:

- Perform a comparative assessment of LAI models (both physical and pre-existing empirical LAI estimation methods) against the ground LAI measurements of the studied crop groups, particularly the newly embedded biophysical processor (based on the ANN method) in the Sentinel Application Platform (SNAP) software, the newly developed S2 LAI algorithm from SeLI index, and the empirical-based HLS-VIs models
- Assess new LAI-VI fits specific to these crop groups
- Establishing crop-specific LAI based biophysical parameters (biomass & crop height) equations, using the Harmonized Satellite data product which involves merging two sensors gridded to a joint pixel resolution, map projection and spatial extent

CHAPTER II

LITERATURE REVIEW

A. LAI Estimation Methods

1. Ground-based LAI Estimation

The indirect measurement of LAI with the optical instruments is based on two major theoretical approaches, namely: the gap fraction or PAR inversion methods. With the gap fraction approach, LAI is determined by solving for L as per the below (Eqs.1 and 2):

$$P(\theta) = e^{-G(\theta,\alpha)\Omega\frac{(\theta)L}{\cos\theta}} \quad (1)$$

$$L = \frac{-(\ln P(\theta)\cos\theta)}{G(\theta)\,\Omega(\theta)} \quad (2)$$

Where P (θ) is the gap fraction, θ is the zenith angle of view, α is the leaf angle, G (θ, α) is the fraction of foliage projected on the plane normal to the zenith direction, and Ω (θ) is the clumping coefficient, When foliage is randomly distributed within the canopy, Ω (θ) = 1, but as the foliage becomes more clumped, Ω (θ) < 1, and L is the Leaf area index. Examples of instruments that use the above theory include the LAI–2200 Plant Canopy Analyzer, which compares above and below canopy light levels detected by five conical rings with zenith view angles ranging from nadir to 75º. Another example is digital hemispherical photography (DHP). DHP measures LAI by the inversion of the Poisson model (Eq.2), as described by Thimonier et al. (2010). DHP uses a fish-eye lens

inside the camera that images the canopy from the beneath in a hemisphere. The collected photographs are then processed by the user using the Can-Eye or other software. By process of thresholding, distinguishing pixels that are occupied by leaves from those that are occupied by the sky, the user can determine the LAI values.

The second approach is based on Beer-Lambert extinction law, and it can be explained as follows: In a case of light absorption by the canopy, according to Beer's law, a relationship between the incident (I_0), transmitted light (I) and leaf area index (L) is given by the below (Eq.3):

Where K is an extinction coefficient which depends on the direction of beam and leaf angle

Distribution. K is calculated, according to Campbell (1986) as per (Eq.4):

$$I = I_0 \times \exp(-K \,.\, L) \tag{3}$$

$$K\,(\times, \theta) = \frac{\sqrt{\times^2 + \tan(\theta)^2}}{\times + 1.72\,(\times + 1.12)^{-0.708}}) \tag{4}$$

Where x is the Ellipsoidal Leaf Angle Distribution (ELADP), and θ is the zenith angle of the direct beam. Typical ELADP values used in this study are summarized in Table 1 from Campbell and Van Evert (1994). A default value of 1 was used for random spherical distribution crops that are not mentioned in the below table 6. Zenith angels are calculated from longitude, latitude, and local timing.

Table 1. Typical ELADP Values

Crop	ELADP
Maize	0.76-2.52
Wheat	0.96
Barley	1.2
Cucumber	2.17
Tobacco	1.29-2.47
Potato	1.7-2.47

Examples of instruments that use the above theory include SS1 SunScan Plant Canopy Analysis System. This instrument consists of 64 PAR sensors with an accuracy of ±10%, embedded in a 1 m long portable probe. Combined with a calibrated BF3 Sunshine Sensor, it measures the incident and transmitted PAR in the canopy to provide an estimate of LAI. A brief theoretical background of how the SunScan computes its reading of LAI can be found in the user's manual. Another instrument is the Accu-PAR model Lp-80 PAR LAI Ceptometer (Decagon Devices, Inc. Pullman, WA, USA). The LAI measured by Accu-PAR and other PAR inversion instruments is dependent on several factors such as the solar zenith angle which is calculated using the time of day and the geographic location, the path length of the beam radiation, and the leaf angle distribution of the canopy as described by Beer's law.

We here present a review of the evaluation of the different LAI instruments. Casa et al. (2019) evaluated different commercial LAI instruments and compared them to direct LAI measurements of different crops. Of these instruments are the LAI-2000, the Sunscan Ceptometer, and the digital hemispherical photography. Casa et al. (2019) concluded that the digital hemispherical photograph provided best estimates of LAI for

alfalfa (RMSE=0.33 m^2/m^2), broad bean (RMSE=0.3 m^2/m^2), emmer (RMSE=0.31 m^2/m^2), maize (RMSE=0.58 m^2/m^2), and wheat (RMSE=0.68 m^2/m^2). Ariza-Carricondo et al. (2019) assessed the LAI–2200 Plant Canopy Analyzer, the SS1 SunScan Canopy Analysis System, and Digital Hemispherical Photography (DHP) for four different canopy types, including maize. The results have shown that LAI-2200 overestimates LAI in a very low range of the directly measured LAI. The DHP only slightly overestimated the direct method, whereas the SS1 underestimated the direct measurements by about 25%; this is consistent with Gower et al. (1999), who showed that SunScan underestimated LAI compared with the destructive measurement. However, the SunScan probe has provided reasonable estimates of leaf area index for corn ($P= 0.0713$) as reported by Wilhelm et al. (2000) and for rice cultivars ($P<0.001$) when restricting the range of LAI to < 4 m^2/m^{-2} as reported by (Sone et al. 2009). Reyes-González et al. (2019) measured the Leaf area index of cornfields with Accu-PAR model Lp-80 PAR LAI Ceptometer (Decagon Devices, Inc. Pullman, WA, USA). In their methodological approach, the LAI measurement was done during the time the satellite overpasses to assess the LAI estimated using the remote sensing-based METRIC model. The results of the comparison of the estimated LAI to the LAI obtained from AccuPAR have shown that LAI values measured in situ were higher than the LAI values estimated using the remote sensing-based METRIC model by about 12%, with a good linear correlation (MBE of 0.61, and RMSE of 0.59). Pasqualotto et al. (2019a) and Anderson et al. (2004) used LAI-2200 Plant Canopy. Pasqualotto et al. (2019a) compared LAI obtained from Sentinel-2 LAI Index SeLI (B8a-B5/ B8a+B5) with the in-situ measurements and found a good linear correlation between them (R2 of 0.732, and RMSE of 0.69 m^2/m^2). Similar results were achieved by Anderson et al.

(2004), where the accuracy of LAI retrieval from Optimized Soil Adjusted Vegetation Index (OSAVI) and Normalized difference Water Index (NDWI) compared to the measured LAI was 0.6 as measured by the root-mean-square-deviation (RMSD).

The previously mentioned stress factors directly affect the light use efficiency (LUE) of the crop, which is defined as the efficiency with which a plant can convert sunlight into dry matter. Both the LUE and stress factors are further described in the next sections.

2. Remote sensing-based LAI Estimation

a. Definition of Remote sensing:

Remote Sensing (RS) is defined as the science of acquiring information about an object from a distance without having direct contact with it (Lillesand 1994). Remote sensing has the potential to provide spatial information on a regional scale and on a real-time basis. In the below subsections, we discuss the methods in which LAI estimation can be done from remote sensing.

b. Multispectral satellites

Multispectral satellites are composed of different bands, spatial and temporal resolution. The wavelength ranges of each band differ from one satellite to the other. A summary of spectral bands is shown in Table 2.

Table 2. Spectral bands and their corresponding wavelengths

	Band	Wavelength (nm)
Visible light	Blue	450–495
	Green	495–570
	Red	620–750
Infrared	Near-Infrared (NIR)	750–900
	Short Wave Infrared (SWIR)	900–3000
	Thermal Infrared (TIR)	3000–14000

i. Landsat 7

Landsat 7 is the seventh satellite of the Landsat series with the enhanced thematic mapper plus (ETM+) sensor(NASA 2016). It was launched on April 15, 1999 (USGS 2017). It has a 16-days temporal resolution. Landsat 7 images are composed of seven shortwave bands of 30 m spatial resolution, and one panchromatic band of 15 m spatial resolution.

ii. Landsat 8

Landsat 8 satellite is the eighth satellite of the Landsat series with the Operational Land Imager (OLI) and the Thermal Infrared Sensor (TIRS) sensors. It was launched on February 11, 2013 (NASA 2013). It has the same temporal resolution as of the Landsat 7. It is composed of nine shortwave spectral bands of 30 m spatial resolution and one panchromatic band of 15 m spatial resolution.

iii. Sentinel-2

Sentinel-2 is a European satellite that provides high-resolution multispectral imagery Launched by the European Space Agency (ESA). Sentinel-2 is composed of two satellites that were launched on June 23, 2015, and March 7, 2017, respectively. Sentinel-2 scenes are composed of 13 shortwave spectral bands of 10, 20, and 60 m spatial resolution.

c. LAI- Spectral Vegetation Indices Approach

Several studies have shown that there is a high correlation between vegetation spectral indices extracted from satellite images and the Leaf Area Index. The plant primarily absorbs the blue and red light and reflects the near-infrared (NIR) and green, explaining the green color of plants (Fig.1). This characteristic is used to develop spectral vegetation indices in remote sensing

Most of the produced indices are calculated from the multispectral satellite images using the red and near infra-red bands. We here present the commonly used vegetation indices:

i. The Normalized difference vegetation index (NDVI) :

Calculated using Eq.5 (Rouse et al. 1974):

$$NDVI = \frac{\rho_{NIR} - \rho_R}{\rho_{NIR} + \rho_R} \quad (5)$$

ii. The soil adjusted vegetation index (SAVI):

Calculated using Eq.6 (Huete 1988):

$$\frac{(1\ +\ L)(\rho_{NIR} - \rho_R)}{\mathrm{L}\ +\ \rho_{\mathrm{NIR}}\ +\ \rho_{\mathrm{R}}} \quad (6)$$

iii. The enhanced vegetation index (EVI2):

Computed using Eq.7 (Kang et al. 2016):

$$2.5\ [\frac{(\rho_{NIR}\ -\ \rho_R)}{(\rho_{NIR} +\ 2.4\ \rho_R) + 1}] \quad (7)$$

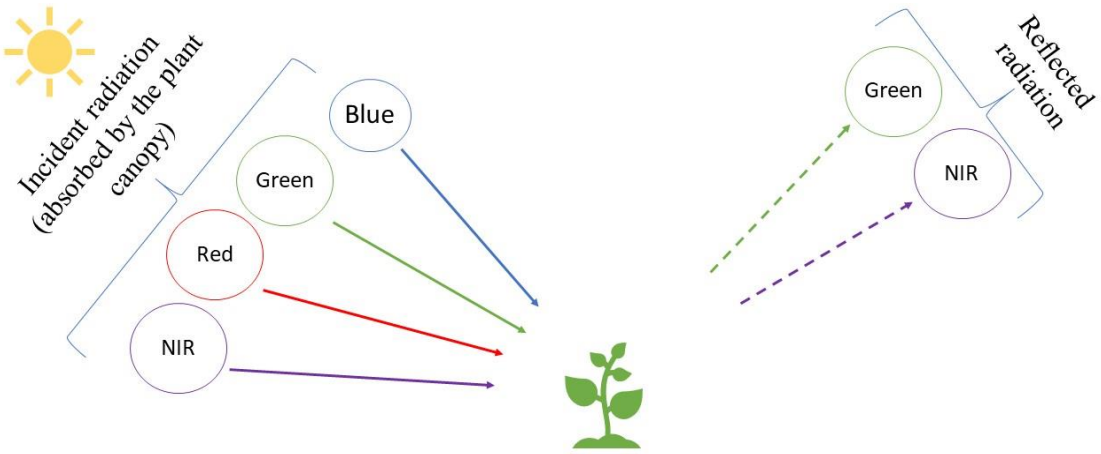

Fig 1. Light interactions at the plant scale Light interactions at the plant scale

The correlation between LAI and the VIs takes various mathematical forms, such as linear, logarithmic, polynomial, or exponential (Nguy-Robertson et al. 2014; Viña et al. 2011b).

d. Physical Modeling Approaches

The physical Modeling approach involves radiation transfer models (RTMs). RTMs provides values of the biophysical variable through modeling the relation between canopy properties and its reflection behavior (Urrutia 2010). The advantages of these models are that they account for the various sources of variability, and LAI can be inverted in the high range, overcoming insensitivity of VI to higher LAI values (González-Sanpedro et al. 2008). The most validated RTMs models to estimate LAI include: the leaf reflectance model, PROSPECT (Jacquemoud and Baret 1990) and canopy reflectance model called SAIL (Verhoef 1985) Examples of the physical modeling technique involves the retrieval of LAI biophysical using biophysical processor tool (Weiss and Baret 2016), implemented ii the Sentinel Application Platform (SNAP), developed by the European Space Agency (ESA).

CHAPTER III

MATERIALS AND METHODS

A. Study area and surveyed crops

The study area is located in the fertile semi-arid Bekaa valley of Lebanon (Fig.2). The climate in the study area is typically the Mediterranean with heavy rains in winter (which extends from December to May) while aridity prevails during the other months of the year (Comair 1998). The rainfall level ranges from 300 mm to 600 mm in the Bekaa Valley in Lebanon. The total agricultural area is 118,000 ha (Jaafar and Ahmad 2020), which accounts for 42 % of the total cultivated area in Lebanon (FAO 2019; MOE 2001). The study area covers Baalbek in the 2019 growing season (characterized by semi-arid climate), and the North to West Bekaa (characterized by the Mediterranean climate) in the 2018 growing season. Field campaigns were conducted to the study area, to acquire ground LAI measurements on different crops. The total number of surveyed fields is 498, with a total area of 4356 ha. A summary statistic on the field campaign carried in the two growing seasons is shown in Fig 3.

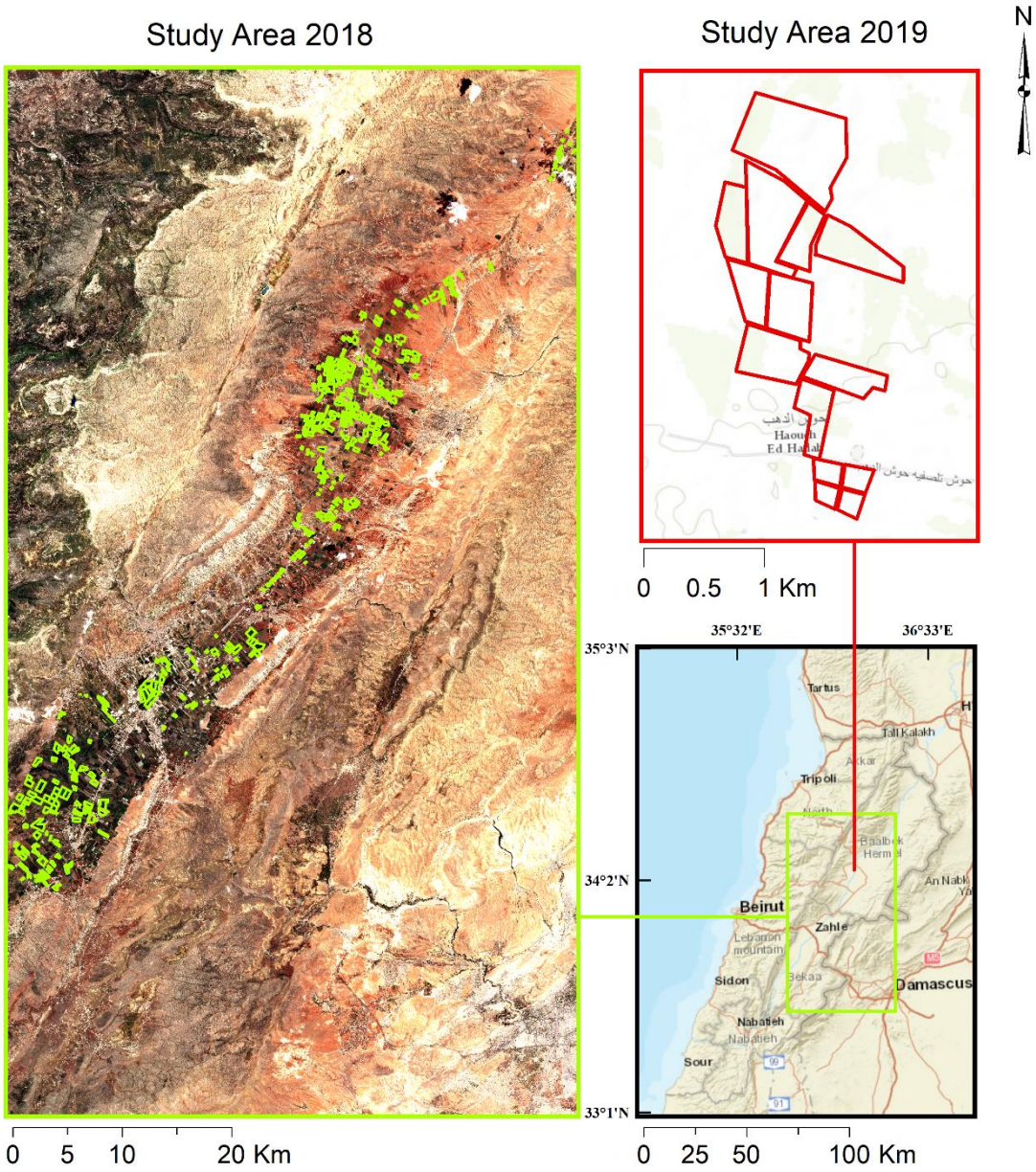

Fig 2. Location of the study area, surveyed fields are outlined in green

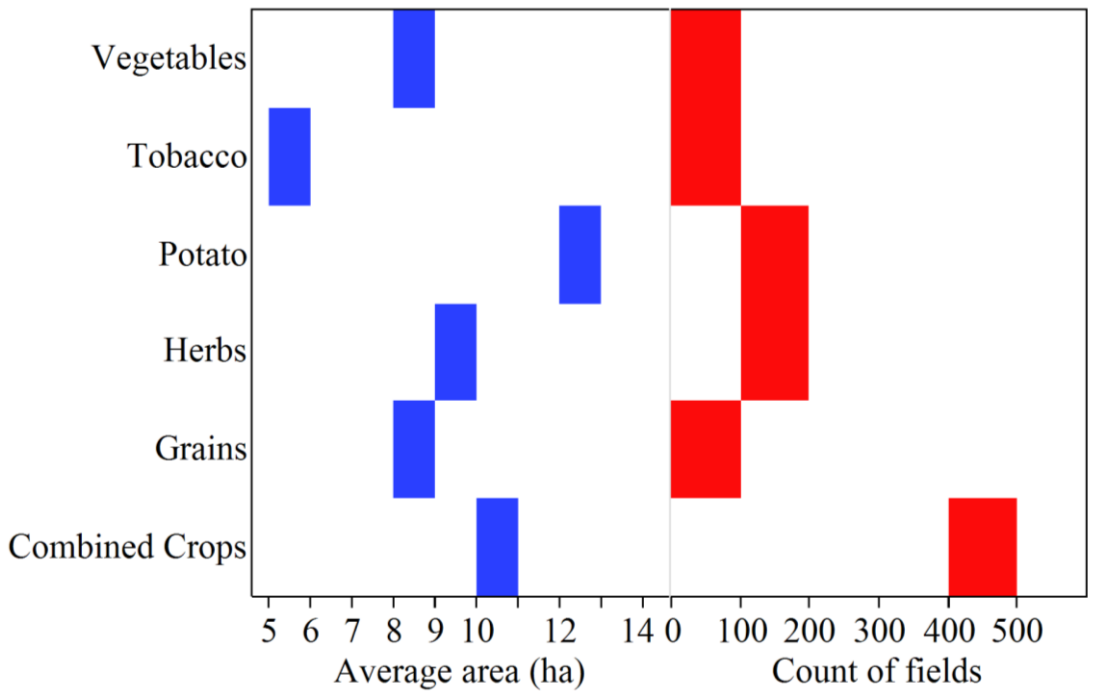

Fig 3. Surveyed crop groups during the 2018-2019 growing seasons, the count of fields and their average area

B. Biophysical Measurements

1. Leaf Area Index Measurements

The in-situ measurements of LAI were conducted using the SS1 SunScan Canopy Analysis System (Delta-T Devices) (Potter et al. 1996). SS1 requires input data, including the Ellipsoidal Leaf Angle Distribution (ELADP), longitude, latitude, and local timing. Typical ELADP values used in this study are summarized in Table 1 in the appendix. LAI measurements were taken during the same period of the satellite overpass to calibrate and validate the relationship between the LAI and vegetation indices.

Two different patterns for data collection were followed during both the growing seasons of 2018 and 2019. In 2018, Leaf Area Index measurements were collected all over the Bekaa Valley. To get around the spatial variability of LAI, we increased our sample size by collecting multiple LAI measurements within the study area. Five measurements were taken from each field, and the average value of the collected measurements was representative of the LAI of the whole field. All the LAI measurement dates coincided with the Landsat and Sentinel data acquisition dates, except for two dates. For each field, random distribution of five LAI measurements at five different locations was taken following an ~ a square grid spatial sampling, ~ 5 m apart (points A, B, C, D, and E) starting from the mid of the field. Measurements were taken away from the field edges to avoid errors that may result in the analysis of a pixel that may contain crop and non-crop signals.

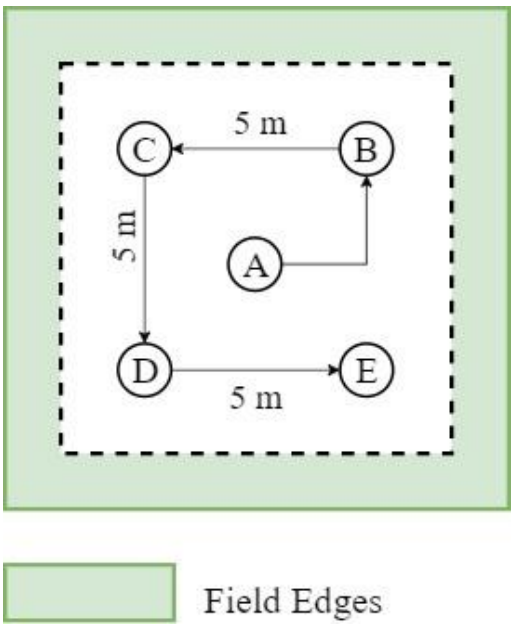

Fig 4. LAI measurement approach for each visited field during 2018 growing season

For the 2019 growing season, extending from April to July, three significant crops were considered including wheat, barley, and potato. The aim was to monitor the LAI dynamics of these crops. A total of 42 predefined sampling sites with GPS coordinates were chosen where LAI was collected from these same locations every time the satellite overpasses. The sampling sites include 21 locations in wheat fields, 12 locations in barley fields, and 9 locations in potato fields. At each sampling site, three LAI measurements were taken and averaged. The sampling locations are shown in Fig 5.

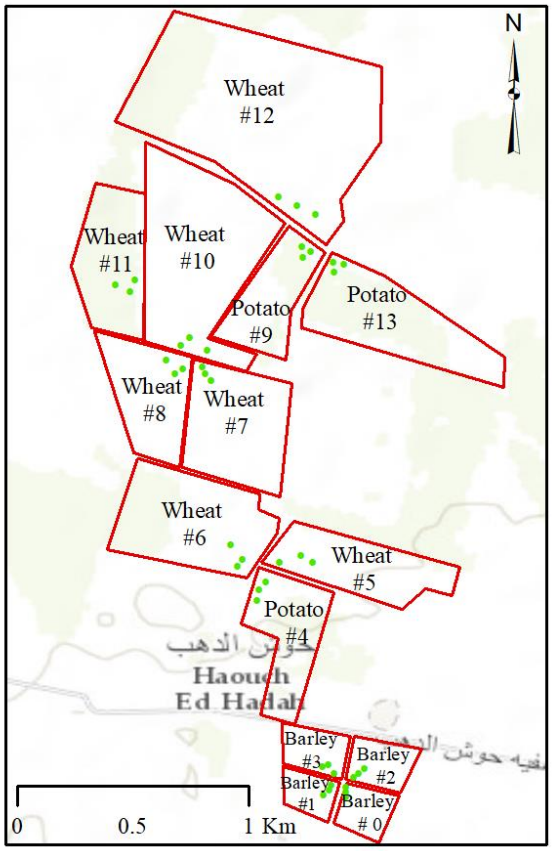

Fig 5. LAI, canopy height, and above-ground biomass sampling sites (labeled in green) for the 2019 growing season

2. Canopy height and Above-ground biomass measurements

Above-ground crop biomass and height measurements were collected from the LAI sampling sites in 2018 and 2019. A quadrate (0.5 m^2 by 0.5 m^2) was randomly thrown in the field, and the vegetation within the frame of the quadrate was clipped. Three samples of the biomass were taken from each field, and the obtained results were averaged. The above-ground plant component was oven-dried at 75 ^{0}C for 48 hours to a constant weight and weighed. Aboveground biomass measurements were conducted for the potato crop in 2019. The crop height was directly measured for the tobacco and cannabis crops in 2018, and potato crop in 2019 for the plant samples within the frame.

C. Surface reflectance data

1. Satellite datasets

A total of 17 HLS images (T36 SYC) were used for the growing season extending from May to September 2018, and a total of 7 images were used for the growing season extending from the end of April to July 2019. Our field visits were organized in a way to meet the time the satellite overpasses. In 2018, we aimed to get as many LAI measurements as possible on different varieties of crops to cover the whole Bekaa agricultural scheme; for this, several HLS scenes were downloaded and used. However, in 2019 we aimed to generate time series from the collected biophysical parameters on only two strategic crops: Potato and Wheat during a different time interval than that of 2018 covering the growing period (planting to harvest) of the Potato crop, where we used fewer HLS scenes but enough to fulfill this aim. Addional 2019 HLS scenes were downloaded and used to generate modeled crop biophysical variables time-series. Fig 6 represents a summary of the obtained satellite data. Atmospherically corrected Level 2- A surface reflectance sentinel-2 (S-2) images were downloaded from the THEIA website at the French Land Data Center (https://www.theia-land.fr/), and they were holding the same dates as S30 from HLS. S-2 images were used to generate LAI using the Sentinel LAI index and SNAP software. We use and validate the newly released harmonized surface reflectance product (HLS, v1.4). HLS represents a synergy of Landsat-8 (L30) and Sentinel-2 (S30) data with 30 meters resolution (Claverie et al. 2018).

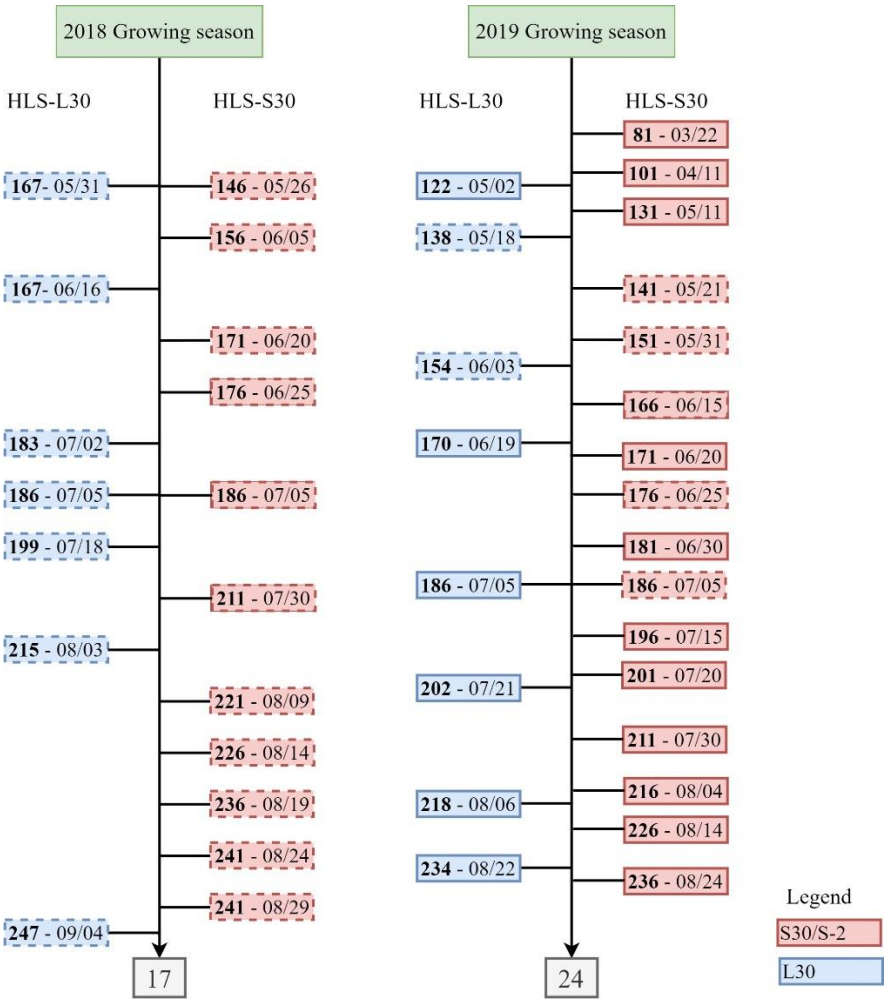

Fig 6. HLS scenes used in the study, Day of the year (DOY) (in bold) with the respective date of HLS products (Landsat 8 (L30) images blue boxes, Sentinel-2 (S30) red boxes) and S2 extracted from THEIA scenes red boxes), with the respective number of total images grey boxes, dashed boxes represent the HLS scenes used to validate LAI, whereas lined boxes are used to generate crop biophysical variable time-series during the 2019 growing season

2. Cloud Masking

Cloud masking is done for acquiring high-quality land surface reflectance values with low uncertainties. The HLS product contains, in addition to the surface reflectance bands, what is referred to as a Level-2-pixel quality assurance band. This band provides

information about the cloud status in each pixel (clear, shadow, low, medium, and high confidence), snow/ice, and water pixels. The Landsat-8 cloud mask is derived from both the mask in the USGS Landsat TOA data and the Land Collection 1 Surface Reflectance Code (LaSRC) atmospheric correction tool. However, the Sentinel-2 cloud mask is a union of the Fmask algorithm, which has been adapted from (Zhu et al. 2015) and the LaSRC mask. The quality assessment band (QA) bits of the HLS Landsat and Sentinel-2 were decoded with a loop using simple integer arithmetic, and its output was used to mask cloud shadow, adjacent cloud, cloud, and cirrus from the processed images.

As for the L2A THEIA's product, it corrects for atmospheric effects and detects the clouds and their shadows using the Multi-sensor Atmospheric Correction and Cloud Screening (MACCS) processor (https://labo.obs-mip.fr/multitemp/?p=6203). The L2A 10-meter cloud mask product was downloaded and used from the mask directory.

3. Vegetation indices

Vegetation indices (VIs) are necessary for the indication of the health and greenness of the vegetation canopy. Vegetation indices are widely used in the assessment of several biophysical parameters including the fraction of photosynthetically active radiation absorbed by the vegetation (FAPAR) (Di Bella et al. 2004), green vegetation fraction (Zeng et al. 2000), leaf area index (LAI) (Boegh et al. 2002), and canopy chlorophyll (Gitelson et al. 2005). In this study, we selected several indices, including Soil adjusted vegetation index (SAVI), Normalized difference vegetation index (NDVI), Enhanced vegetation index 2 (EVI2), and Sentinel-2 LAI Index (SeLI) to be used for the evaluation of LAI. SAVI, NDVI, and EVI2 are a combination of visible and near-infrared bands. While SeLI is a combination of near-infrared and red edge bands of the sentinel2 imagery. In literature, it is common that the vegetation indices are calculated from top-of-atmosphere reflectance. In our application, we calculate the VIs (NDVI, SAVI, and EVI2) using the HLS (Harmonized Landsat Sentinel-2) 30-m products consisting of surface reflectance derived from both Landsat-8 L1T products and Sentinel-2 MSI L1C data. Furthermore, we calculated SeLI from the L2A THEIA surface reflectance product. SeLI is a new robust LAI_{green} index developed by Pasqualotto et al. (2019a) computed from near-infrared and red edge bands. The red-edge region, between 690 and 750 nm, represents the region between the maximum absorption in the red wavelength and maximum reflection in the near-infrared wavelength, by the plant (Guyot et al. 1992; Liu et al. 2004). Several researchers emphasize the importance of the red edge band in the estimation of LAI_{green}. NDVI was selected as one of the simplest and earliest VI. Compared to NDVI, SAVI and EVI2 are less sensitive to soil background (Kang et al. 2016). However, the disadvantages of

SAVI, NDVI, and EVI2 is that they tend to saturate at moderately high LAI (~ 2.5-3). For SAVI, we use L=0.5 (USGS, 2017b). Equations of the used VIs, along with their references, are presented in Table 3.

Table 3. References and equations of selected VIs to be evaluated in this study

Index	Acronym	Equation	Reference
Soil adjusted vegetation index	SAVI	$\frac{(1 + L)(\rho_{NIR} - \rho_R)}{L + \rho_{NIR} + \rho_R}$	(Huete 1988)
Normalized difference vegetation index	NDVI	$\frac{\rho_{NIR} - \rho_R}{\rho_{NIR} + \rho_R}$	(Rouse Jr et al. 1974)
Enhanced vegetation index 2	EVI2	$2.5\ [\frac{(\rho_{NIR} - \rho_R)}{(\rho_{NIR} + 2.4\ \rho_R) + 1}]$	(Kang et al. 2016)
Sentinel-2 LAI Index	SeLI	$\frac{\rho_{NIR2} - \rho_{Red\ Edge\ 1}}{\rho_{NIR2} + \rho_{Red\ Edge\ 1}}$	(Pasqualotto et al. 2019a)

D. LAI Models

1. Existing VI-based LAI models

We used existing LAI models to create spatial LAI layers of the study area. These models are evaluated and validated with the collected LAI measurements to determine the best fit model. We analyzed the LAI obtained from NDVI with linear, exponential, and polynomial of third-order fittings. We also analyzed LAI obtained

from SAVI with a polynomial of third order and logarithmic fittings, LAI obtained from EVI2 with square root fittings, and LAI obtained from SeLI with a linear fitting. To be able to compare the LAI derived from LAI models as they exist in literature against the ground-based LAI measurements, we used the zonal statistics tool for the 2018 growing season, and the extract multi-value to point tool for the 2019 growing season. The relationships between LAI and different studied vegetation indices, as presented in Literature, are summarized in Table 4.

Table 4. References and equations of selected existing VI-based LAI models to be evaluated in this study

Model #	Relation	Equation of LAI	Studied Crop	Satellite	Reference
1	LAI-NDVI	$4.9\mathrm{NDVI} - 0.46$	Vineyard	Multi-spectral imagery obtained from IKONOS	(Johnson et al., 2003)
2		$0.0287\ e^{5.081\mathrm{NDVI}}$	Wheat and Corn	L5 TM	(González Piqueras, 2006)
3		$9.519 \times \mathrm{NDVI}^3 - 0.104 \times \mathrm{NDVI}^2 + 1.236 \times \mathrm{NDVI} - 0.257$	Overall vegetation cover & crops		(Myneni et al. 1997)
4	LAI-SAVI	$11 \times \mathrm{SAVI}^3$	Overall vegetation cover, woody trees, &agricultural crops	L5 TM & L7 ETM+	(Pôças et al., 2014)
5		$\frac{-\ln\left(\frac{0.69 - \mathrm{SAVI}}{0.59}\right)}{0.91}$			
6	LAI-EVI2	$\left(2.92\sqrt{\mathrm{EVI2}} - 0.43\right)^2$	Overall crops	Atmospherically corrected L5 TM & L7 ETM+	(Kang et al., 2016a)
7		$\left(3.16\sqrt{\mathrm{EVI2}} - 0.58\right)^2$	Row crops		
8		$\left(5.3\sqrt{\mathrm{EVI2}} - 1.66\right)^{2/3}$	Maize		

Model #	Relation	Equation of LAI	Studied Crop	Satellite	Reference
9		$(5.47\ \mathrm{EVI2}^{\frac{3}{5}} - 1.03)^{4/3}$	Wheat		
10	SeLI (Sentinel-2 LAI index)	$5.405 \times \mathrm{SeLI}\text{-}0.114$	Overall crops (potato, artichoke, squash, alfalfa, lettuce, wheat, pumpkin, & others)	Atmospherically corrected Sentinel-2 Surface reflectance	(Pasqualotto et al. 2019a)

2. SNAP Model

In addition to the generation of LAI from the relationship with the vegetation indices, LAI was produced from S2 THEIA surface reflectance data using Sentinel Application Platform toolbox (SNAP) software. SNAP provides a scientific processor tool named "Biophysical Processor," in the Thematic Land Processing pull-down menu, for the retrieval of several biophysical parameters including LAI. The principle is to retrieve LAI from Sentinel-2 scenes using the algorithm implemented in the SNAP software, which is based on neural networks that are trained to estimate the canopy characteristics (Bochenek et al. 2017). LAI can be directly retrieved for each pixel based on a pre-trained neural net. The neural nets are trained using well known RTM (PROSAIL: PROSPECT (Jacquemoud and Baret 1990) +SAIL (Féret et al. 2017)) as described in (Weiss and Baret 2016). The ANN algorithm hereby requires the input of eight S2 spectral wavebands (B3–B7, B8a, B11, and B12) which are all resampled to 20 m, in order to preserve the red-edge region in the S-2 scenes. LAI, with the quality indicators of the used dataset, were thus automatically obtained with the finest possible

resolution. To reduce the processing time and image size, we extracted the area corresponding to the bounding box of the shapefile.

Fig 7 represents a summary of the overall methodological approach that was followed in this study to generate LAI from the studied vegetation indices, L2A THEIA's product, and SNAP software.

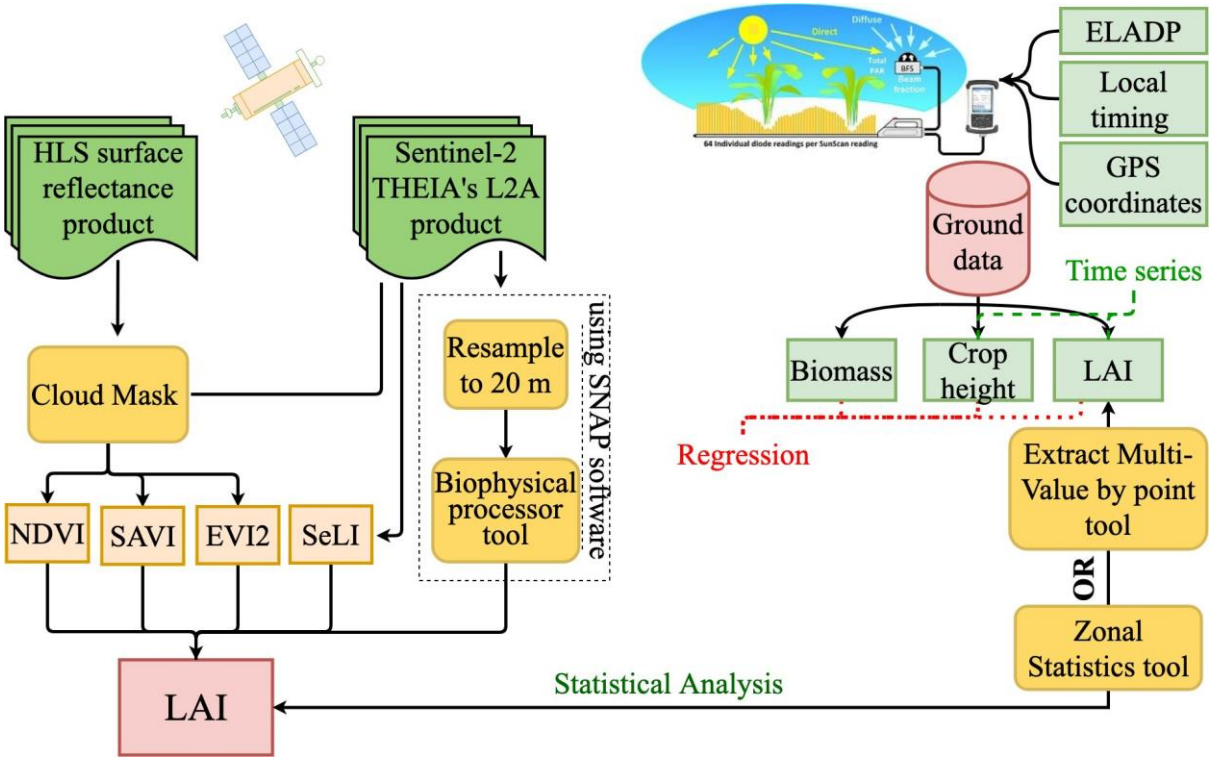

Fig 7. Step-by-step flow chart for the validation of satellite-derived LAI against the ground measured LAI

E. Accuracy Assessment

Statistical analysis between ground measured LAI and remotely sensed LAI derived from S-2 and HLS product was performed for each crop group during the 2018-2019

growing seasons. This analysis aimed to evaluate the accuracy of each LAI model and to determine which indices are the best fit to remotely sensed LAI estimation. In 2018, the study was conducted on five crop groups, namely: Herbs (Cannabis: *Cannabis sativa,* Mint: *Mentha,* Onion: *Allium cepa,* Parsley: *Petroselinum crispum*), Grains (Barley: *Hordeum vulgare* and Wheat: *Triticum aestivum*), Potato: *Solanum tuberosum*, Tobacco: *Nicotiana tabacum,* and Vegetables (Bean: *Phaseolus vulgaris,* Cabbage: *Brassica oleracea,* Carrot: *Daucus carota subsp. sativus,* Chickpea: *Cicer arietinum* , Corn: *Zea mays*, Cucumber: *Cucumis sativus*, Lettuce: *Lactuca sativa*, Eggplant: *Solanum melongena*, Melon: *Cucumis melo var. cantalupensis*, and Pepper: *Capsicum annuum*). In 2019, the study was conducted on three major crops, namely: Wheat, Barley, and Potato. Statistical analysis was based on RMSE (Eq.8), MAE (Eq.9), and MAPE (Eq.10), RRMSE (Eq.11), Mean Bias Error (MBE) (Eq.12) and d (Eq.13) as follows:

Root Mean Square Error (RMSE):

$$\mathrm{RMSE} = \sqrt{\frac{\sum_{i=1}^{n}(\mathrm{Estimated\ LAI_i} - \mathrm{Measured\ LAI_i})^2}{n}} \tag{8}$$

Mean Absolute error (MAE):

$$\mathrm{MAE} = \frac{\sum_{i=1}^{n}|\mathrm{Estimated\ LAI_i} - \mathrm{Measured\ LAI_i}|}{n} \tag{9}$$

Mean absolute percentage error (MAPE):

$$\mathrm{MAPE} = \frac{1}{n}\sum_{i=1}^{n}\frac{\left|(\mathrm{Measured\ LAI_i} - \mathrm{Estimated\ LAI_i})\ \right|}{\mathrm{Measured\ LAI_i}} \tag{10}$$

Relative RMSE:

$$\mathrm{RRMSE} = \frac{\mathrm{RMSE}}{\overline{\mathrm{Measured\ LAI_\iota}}} \times 100 \tag{11}$$

Mean Bias Error (MBE):

$$\mathrm{MBE} = \frac{\sum_{\mathrm{i=1}}^{\mathrm{n}}(\mathrm{Estimated\ LAI_i} - \mathrm{Measured\ LAI_i})}{\mathrm{n}} \tag{12}$$

Index of agreement (d):

$$\mathrm{d} = 1 - \frac{\sum_{\mathrm{i=1}}^{\mathrm{n}}(\mathrm{Measured\ LAI_i} - \mathrm{Estimated\ LAI_i})^2}{\sum_{\mathrm{i=1}}^{\mathrm{n}}(\left|\mathrm{Estimated\ LAI_i} - \overline{\mathrm{Measured\ LAI_\iota}}\right| + \left|\mathrm{Measured\ LAI_i} - \overline{\mathrm{Measured\ LAI_\iota}}\right|)^2} \tag{13}$$

We also investigate the relation between the measured LAI and the remotely sensed vegetation indices. For this purpose, we use Pearson's r, which is the most used parametric correlation coefficient, and it is given by Eq. 14:

$$\mathrm{r} = \frac{\sum_{\mathrm{i}}(\mathrm{x_i} - \overline{\mathrm{x}})(\mathrm{y_i} - \overline{\mathrm{y}})}{\sqrt{\sum_{\mathrm{i}}(\mathrm{x_i} - \overline{\mathrm{x}})^2\sqrt{(\mathrm{y_i} - \overline{\mathrm{y}})^2}}} \tag{14}$$

The significance is computed using the two-tailed t-test with n-2 degrees of freedom

$$\mathrm{t} = \mathrm{r}\sqrt{\frac{\mathrm{n}-2}{1-\mathrm{r}^2}} \tag{15}$$

CHAPTER IV

RESULTS

The performance of the empirical and biophysical models was evaluated using the aforementioned statistical parameters when compared to field measurements. A table of the performed statistical analysis, along with a summary graphical representation, is shown in Fig 8&9 and table 5 &6, respectively. The conclusions that were drawn from our study are explained in the below sections.

A. Evaluation of existing LAI Models

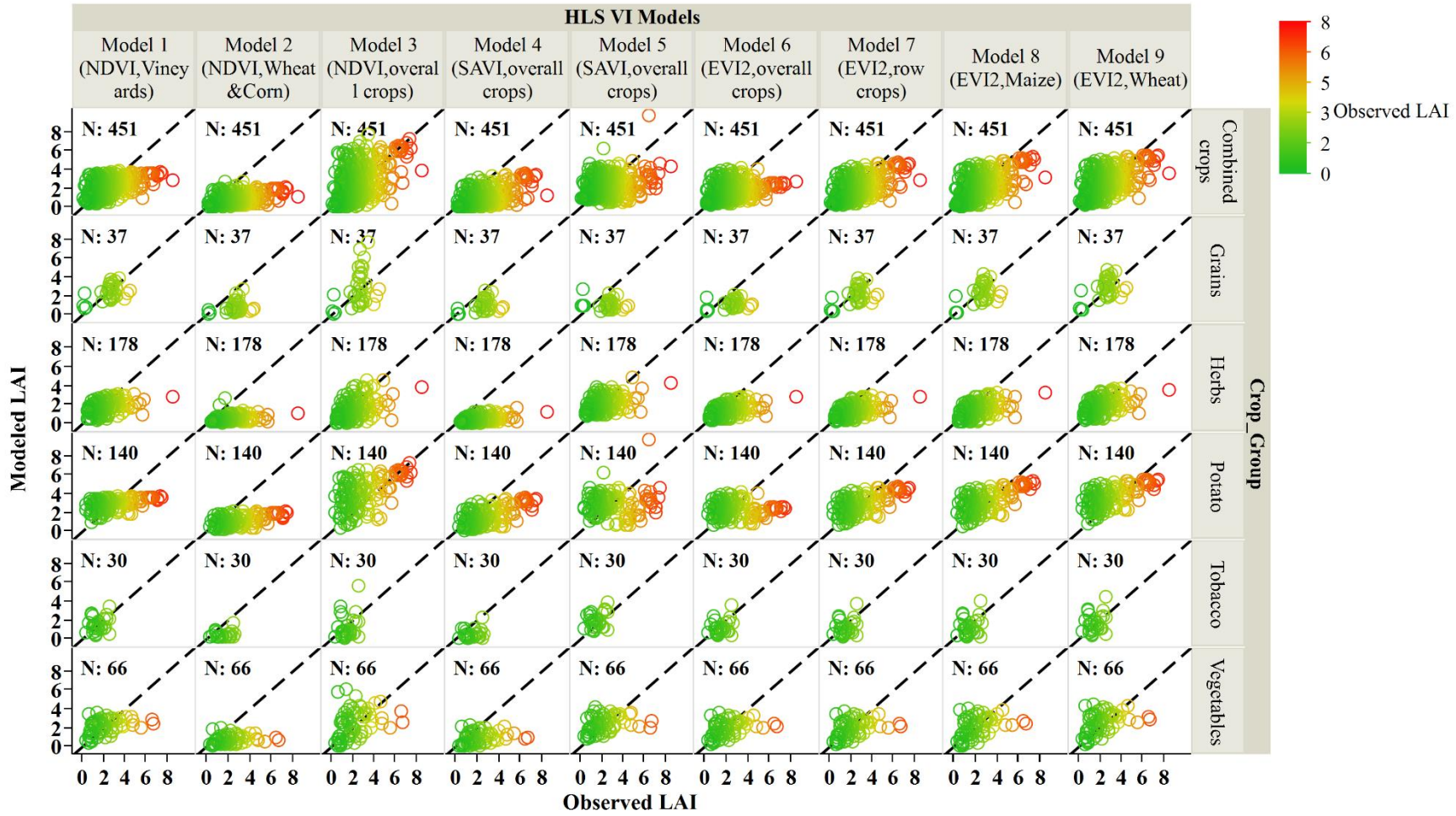

Fig. 8. Comparison between modeled and observed LAI in the 2018-2019 growing seasons for the HLS-VI Models, the color bar represents the measured LAI ranges, divided into low (0-2 m^2/m^2), medium (2-4 m^2/m^2), and high (>4 m^2/m^2) LAI range

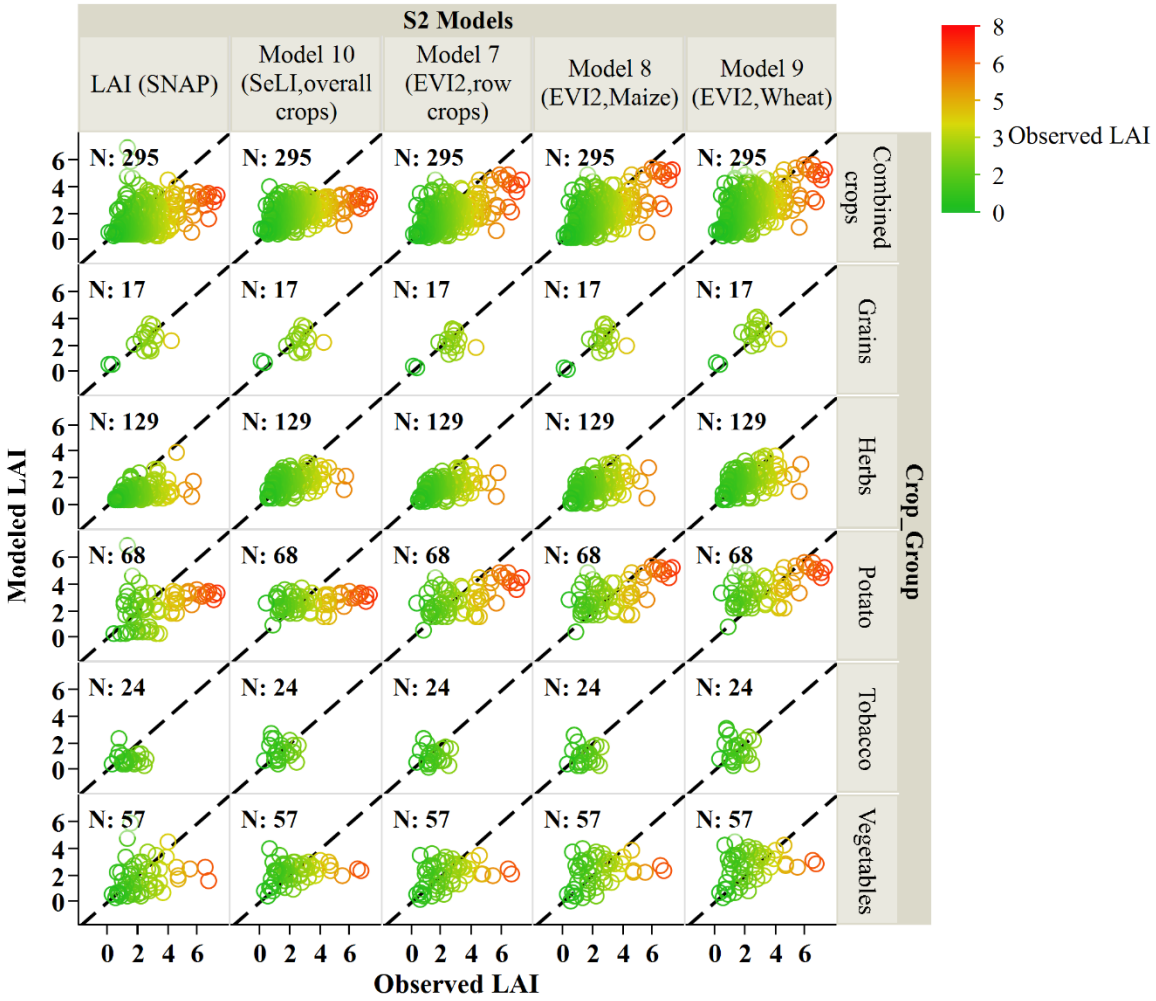

Fig 9. Comparison between modeled and observed LAI in the 2018-2019 growing seasons for the HLS-VI for the HLS VI best-performing Models derived from S30, Model 10 (SeLI, overall crops) and SNAP Model derived from S2 THEIA Product; the color bar represents the measured LAI ranges, divided into low (0-2 m2/m2), medium (2-4 m2/m2), and high (>4 m2/m2) LAI range

Table 5. Statistical analysis summary for the studied crops in both 2018 and 2019 growing seasons for the vegetation indices derived from the HLS product Models

HLS VI Models

LAI Model	Statistical Parameter	Herbs (n=178)	Potato (n=140)	Tobacco (n=30)	Vegetables (n=66)	Grains (n=37)	Combined Crops (n=451)
Model 1 (NDVI, Vineyard)	MAE	0.82	1.28	0.64	0.98	0.74	0.97
	RMSE	1.19	1.60	0.83	1.32	0.94	1.31
	RRMSE	55%	55%	54%	59%	37%	55%
	MAPE	39%	64%	52%	54%	66%	52%
	MBE	-0.43	-0.09	-0.06	-0.11	-0.26	-0.24
	d	0.66	0.50	0.66	0.57	0.69	0.63
Model 2 (NDVI, Wheat & Corn)	MAE	1.76	1.87	1.21	1.65	1.88	1.76
	RMSE	2.07	2.40	1.35	2.09	2.10	2.16
	RRMSE	97%	82%	88%	94%	82%	90%
	MAPE	80%	59%	76%	71%	72%	71%
	MBE	-1.74	-1.81	-1.21	-1.60	-1.86	-1.72
	d	0.45	0.50	0.39	0.47	0.40	0.48
Model 3 (NDVI, Overall agricultural crops)	MAE	1.01	1.56	1.03	1.25	1.41	1.25
	RMSE	1.35	1.95	1.26	1.67	1.77	1.64
	RRMSE	63%	67%	82%	75%	69%	68%
	MAPE	48%	95%	75%	75%	73%	70%
	MBE	-0.66	1.99	-0.34	0.12	0.09	0.05
	d	0.74	0.70	0.75	0.59	0.51	0.71
Model 4 (SAVI, Overall agricultural crops)	MAE	1.75	1.58	1.16	1.50	1.72	1.62
	RMSE	2.06	1.97	1.30	1.95	1.96	1.97
	RRMSE	96%	68%	84%	88%	76%	82%
	MAPE	80%	55%	75%	66%	70%	69%
	MBE	-1.75	-1.39	-1.12	-1.41	-1.70	-1.54
	d	0.47	0.60	0.47	0.48	0.47	0.54
Model 5 (SAVI, Overall agricultural crops)	MAE	0.82	1.68	0.69	1.02	1.82	1.19
	RMSE	1.12	2.09	0.88	1.40	1.97	1.59
	RRMSE	52%	72%	57%	63%	77%	66%
	MAPE	43%	80%	80%	60%	117%	64%
	MBE	-0.13	-0.05	0.34	0.09	-1.58	-0.16
	d	0.63	0.39	0.52	0.55	0.31	0.52
Model 6 (EVI2, Overall agricultural crops)	MAE	0.94	1.55	0.72	1.00	1.59	1.18
	RMSE	1.33	2.08	0.88	1.37	1.76	1.62
	RRMSE	62%	71%	57%	61%	68%	68%
	MAPE	39%	63%	53%	51%	81%	53%
	MBE	-1.46	-0.61	-0.77	-0.38	-1.47	-0.71
	d	0.54	0.35	0.53	0.58	0.42	0.49

HLS VI Models							
LAI Model	Statistical Parameter	Herbs (n=178)	Potato (n=140)	Tobacco (n=30)	Vegetables (n=66)	Grains (n=37)	Combined Crops (n=451)
Model 7 (EVI2, row crops)	MAE	0.96	1.14	0.77	1.01	0.84	1.00
	RMSE	1.35	1.42	0.92	1.38	1.10	1.34
	RRMSE	63%	49%	60%	62%	43%	56%
	MAPE	41%	57%	55%	52%	52%	49%
	MBE	-0.85	-0.12	-0.38	-0.37	-0.52	-0.5
	d	0.59	0.72	0.52	0.59	0.66	0.70
Model 8 (EVI2, Maize)	MAE	0.94	1.15	0.80	1.02	0.85	1.00
	RMSE	1.31	1.41	0.99	1.38	1.08	1.32
	RRMSE	61%	48%	65%	62%	42%	55%
	MAPE	42%	64%	58%	57%	51%	53%
	MBE	-0.78	0.16	-0.33	-0.21	-0.35	-0.34
	d	0.59	0.76	0.52	0.62	0.68	0.73
Model 9 (EVI2, Wheat)	MAE	0.80	1.29	0.76	1.05	0.85	0.99
	RMSE	1.12	1.56	0.99	1.40	1.03	1.30
	RRMSE	52%	44%	65%	63%	40%	54%
	MAPE	40%	78%	63%	66%	67%	59%
	MBE	-0.33	0.62	0.09	0.23	0.16	0.11
	d	0.66	0.72	0.60	0.64	0.69	0.74

Table 6. Statistical analysis summary for the studied crops in both 2018 and 2019 growing seasons for the HLS VI best-performing Models derived from S30, Model 10 (SeLI, overall crops) and SNAP Model derived from S2 THEIA Product

S2 Models							
LAI Model	Statistical Parameter	Herbs (n=129)	Potato (n=68)	Tobacco (n=24)	Vegetables (n=57)	Grains (n=17)	Combined Crops (n=295)
Model 10 (SeLI, THEIA S2, Overall agricultural & row crops)	MAE	0.82	1.44	0.69	1.01	0.70	0.98
	RMSE	1.21	1.85	0.86	1.40	0.89	1.38
	RRMSE	55%	56%	59%	59%	35%	59%
	MAPE	36%	52%	58%	55%	51%	46%
	MBE	-0.49	-0.69	-0.11	-0.19	-0.36	-0.44
	d	0.56	0.43	0.42	0.51	0.73	0.58
LAI-SNAP (THEIA S2)	MAE	1.24	1.80	0.93	1.28	0.65	1.32
	RMSE	1.61	2.19	1.08	1.73	0.83	1.72
	RRMSE	73%	66%	73%	73%	33%	70%

S2 Models							
LAI Model	Statistical Parameter	Herbs (n=129)	Potato (n=68)	Tobacco (n=24)	Vegetables (n=57)	Grains (n=17)	Combined Crops (n=295)
	MAPE	52%	63%	61%	59%	37%	56%
	MBE	-1.21	-0.98	-0.75	-0.60	-0.27	-0.95
	d	0.54	0.50	0.37	0.52	0.78	0.59
Model 7 (EVI2, HLS VI, row crops)	MAE	1.00	1.17	0.83	1.10	0.65	1.02
	RMSE	1.39	1.50	0.98	1.46	0.91	1.38
	RRMSE	63%	45%	66%	62%	36%	57%
	MAPE	41%	46%	62%	55%	31%	46%
	MBE	-0.91	-0.43	-0.43	-0.37	-0.47	-0.63
	d	0.56	0.70	0.37	0.55	0.75	0.69
Model 9 (EVI2, HLS VI, Wheat)	MAE	0.79	1.21	0.78	1.14	0.70	0.95
	RMSE	1.14	1.47	1.02	1.49	0.83	1.27
	RRMSE	52%	37%	69%	63%	33%	52%
	MAPE	36%	60%	70%	68%	44%	51%
	MBE	-0.40	0.32	0.003	0.26	0.21	-0.04
	d	0.64	0.73	0.40	0.60	0.79	0.74
Model 8 (EVI2, HLS VI, Maize)	MAE	0.97	1.12	0.86	1.11	0.64	1.01
	RMSE	1.35	1.40	1.04	1.47	0.87	1.34
	RRMSE	62%	42%	71%	62%	35%	55%
	MAPE	42%	50%	65%	60%	27%	48%
	MBE	-0.85	-0.12	-0.41	-0.18	-0.30	-0.48
	d	0.60	0.76	0.37	0.57	0.79	0.73

1. HLS VI Models

Empirical LAI models that are developed in relation to the vegetation indices are considered as one of the most straightforward methods used for predicting LAI. We here evaluated the efficiency and robustness of LAI models developed from indices that are computed from red and near-infrared HLS surface reflectance bands using the Normalized Difference ratio: NDVI (Model 1, 2, and 3), Soil Adjusted Vegetation Index: SAVI (Model 4 and 5), and Enhanced Vegetation index 2: EVI2 (Model 6, 7, 8,

and 9). Our analysis shows that Model 7 (EVI2, row crops), Model 9 (EVI2, wheat), and Model 8 (Maize, EVI2) outperformed other models for the crops combined. The accuracy results from the HLS VIs models were better than that derived from S2 SeLI and SNAP model, placing the recently available HLS product at an advantage over SeLi and SNAP Models. Also, LAI derived from EVI2 outperformed the LAI Models derived from the other studied vegetation indices.

On the other hand, further conclusions on the models that performed worst can be deduced from the conducted analysis. Both Models 2 (NDVI, wheat, and corn) and 4 (SAVI, overall agricultural crops) underestimated the LAI for all crops. Underestimation was also noticed in Models 5 (SAVI, overall agricultural crops) and Model 6 (EVI2, overall agricultural crops) for grains. Models 8 (EVI2, maize) and 3 (NDVI, overall agricultural crops) overestimated the LAI for potato.

2. S2 SeLI Model

We here assess the performance of the newly developed LAI algorithm from SeLI. In their study, Pasqualotto et al. (2019a) showed that LAI derived SeLI could be used as a generic model for LAI_{green} of different crop types. Our results agree with the conclusions obtained by Pasqualotto et al. (2019a) and Sharma et al. (2015), who pointed out that the S2 bands located in the red-edge region are recognized as crucial bands for the estimation of the biophysical variables, principally the LAI. Where, Model 10 (SeLI, overall agricultural crops) was one of the best performing models for the crops combined since it comes in the second step following the HLS-VI in terms of low errors. Thus, the red-edge bands used in the S2 SeLI LAI algorithm offers an

improved LAI crop biophysical parameter retrieval with approximately the same accuracy level of HLS-EVI2 Models 7 and 9.

3. SNAP Model

Our assessment shows that LAI derived from SNAP performed the best for grains crop group as compared to HLS VI and S2 SeLI Models. The results demonstrate the potential of using SNAP to derive accurate LAI estimations for both Wheat and Barley. A clear underestimation of the LAI SNAP product was noticed for herbs, potato, vegetables, and tobacco. Our results are consistent with those obtained by Bochenek et al. (2017), who showed that LAI estimation from SNAP software was generally underestimated. Also, Pasqualotto et al. (2019a) showed that LAI estimated from Sentinel-2 product using the SNAP software showed a clear underestimation in the studied crops, including potato, artichoke, squash, alfalfa, lettuce, wheat, pumpkin, & others. Our results indicate that SNAP provided less accurate estimations than HLS-VI and S2 SeLI Models.

B. Empirical relationships between VIs and LAI observations in Bekaa

The performance of the studied indices derived from the HLS product was evaluated using the multi-crop dataset collected over both 2018 and 2019 growing seasons. The semi-empirical relationships between the measured LAI and the vegetation indices for all combined crops and different crop groups are given in Tables A1 and A2 in the Appendix, respectively. The different types of fitting functions had an R^2 ranging between 0.21 and 0.6, with a quadratic and crop group-specific LAI-VIs relationship.

The accuracies of each index obtained with different fittings were moderate except for the SeLI index. However, the p-value was <0.0001 in all cases. Results for Pearson's r correlation shows a strong correlation between the measured LAI and EVI2 (r = 0.7), followed by SAVI (r = 0.67) and NDVI (r = 0.6) and SeLI (r=0.5) with the lowest correlation. Each index was represented as a function of the measured LAI for the different crop groups and the combined crops (Fig.10). However, the EVI2 index hereby can be identified as a best-suited index for a unified algorithm for the crops combined.

More promising results were obtained when evaluating the performance of the vegetation indices for each crop group separated by the satellite type. An R^2 ranging between 0.2 and 0.8 was obtained for the best performing index (EVI2) in each crop group, with the highest R^2 was seen in HLS-L30.

The major challenge of retrieving LAI from vegetation indices is the difficulty of finding one index with a general character that it can be used to estimate LAI for a wide variety of crop types. Where in this work, the established indices do not present this general character; each index performed differently in different crop types. The most robust relation between ground measured LAI and vegetation indices appears in SeLI for cannabis, SAVI, and EVI2 for potato, NDVI for tobacco, EVI2 for vegetables, but EVI2 performed best over most of the crop types. A drawback of the studied indices identified in this study is that they all presented a saturation problem at high LAI values in both grains and tobacco crop groups.

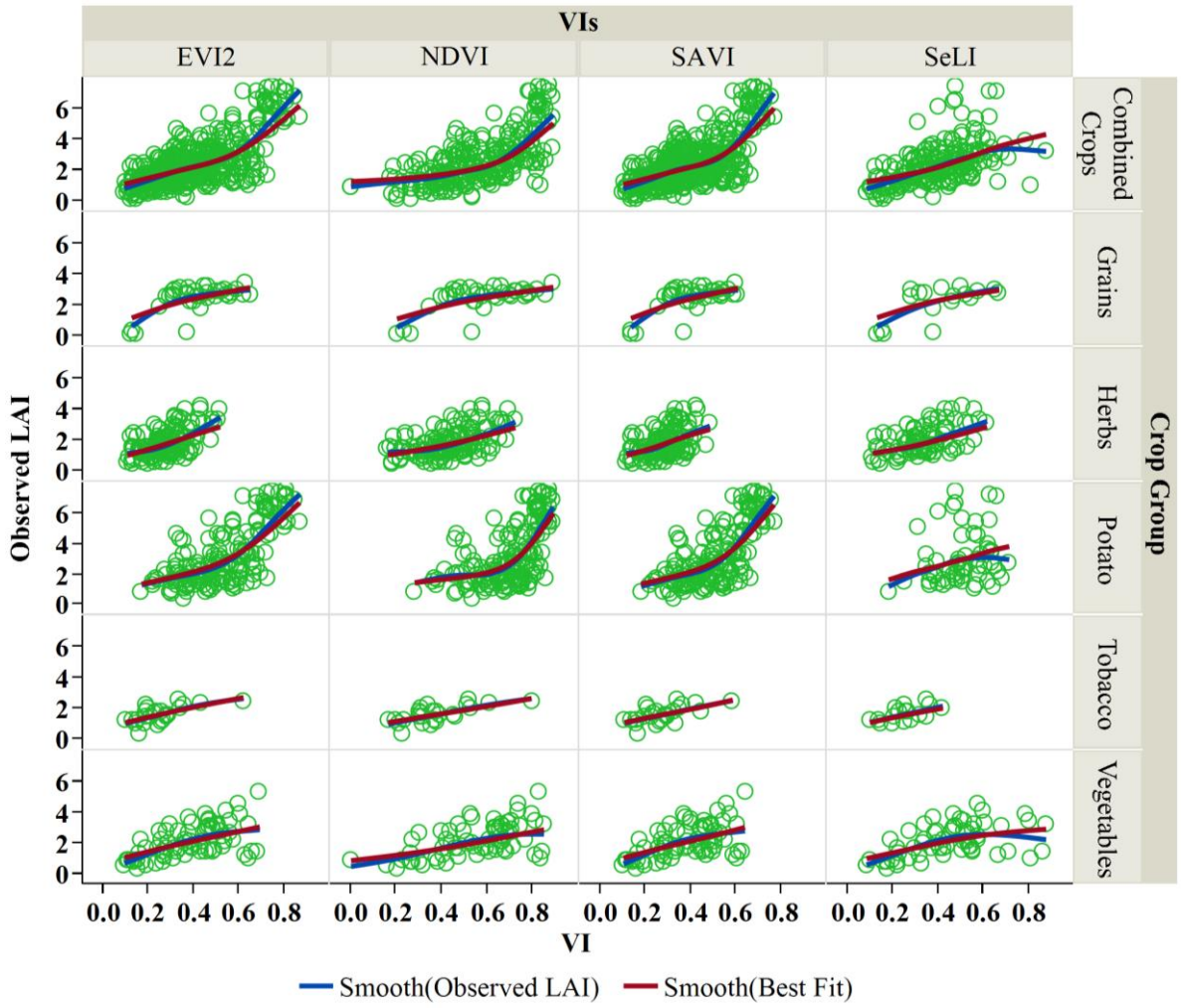

Fig. 10. Measured LAI as a function of vegetation indices (VI) derived from HLS product for the different studied crop groups and all crops combined

Table 7. Statistics obtained using regression equations of the form y= (a *VI + b) * (1+c * exp [d* VI]) for each of the studied index, for the studied crop groups.

Crop Group	VI	Regression Coefficients				P-value	RMSE	R2
		a	b	c	d			
Grains	EVI2	5.002	-0.6	14.9	-7.001	<.0001	0.54	0.63
	SAVI	1.7	4.0	-0.9	-1.7	<.0001	0.63	0.63
	NDVI	1.6	2.1	-0.4	-1.4	<.0001	0.68	0.60
	SeLI	1.7	3.1	-0.8	-1.2	0.003	0.84	0.60
Potato	EVI2	3.0	0.6	0.02	5.1	<.0001	1.29	0.57
	SAVI	3.5	0.4	0.01	6.5	<.0001	1.28	0.57
	NDVI	-3.4	3.4	0.0002	12.8	<.0001	1.38	0.49
	SeLI	0.2	0.0	80.8	-1.9	0.046	1.59	0.06
Herbs	EVI2	-1.1	0.8	0.3	7.3	<.0001	0.69	0.34
	SAVI	1.1	0.2	1.6	1.3	<.0001	0.74	0.23
	NDVI	1.6	2.4	-0.9	-1.7	<.0001	0.73	0.29
	SeLI	1.0	0.3	1.3	1.1	<.0001	0.69	0.32
Tobacco	EVI2	0.009	0.002	367.0	0.0	0.0004	0.40	0.43
	SAVI	0.009	0.002	347.7	0.0	0.001	0.43	0.37
	NDVI	0.009	0.002	302.0	0.0	<.0001	0.37	0.50
	SeLI	0.009	0.002	369.9	0.0	0.006	0.35	0.39
Vegetables	EVI2	0.04	0.006	96.2	0.0	<.0001	0.86	0.33
	SAVI	0.02	0.003	176.9	0.0	<.0001	0.88	0.30
	NDVI	0.1	0.03	22.7	0.0	<.0001	0.91	0.26
	SeLI	0.003	0.001	865.3	0.0	0.0001	0.90	0.32
Combined Crops	EVI2	2.9	0.8	0.012	5.5	<.0001	1.00	0.58
	SAVI	3.2	0.7	0.003	7.9	<.0001	1.01	0.56
	NDVI	1.0	1.1	0.013	5.7	<.0001	1.03	0.55
	SeLI	1.1	0.0	4.9	-0.6	<.0001	1.00	0.31

C. Using VIs to monitor crop development in the Bekaa Valley

1. Using LAI and VI to infer plant growth variables

VIs are among the oldest tools in remote sensing used to estimate a wide variety of plant growth variables. We here studied how good the studied vegetation indices

(SeLI, SAVI, NDVI, and EVI2), modeled LAI (from two best performing models, Models 7,9 and 10), and the observed LAI are correlated to the observed height and above-ground biomass of the four crop groups: Potato, Wheat, Cannabis, and Tobacco. Results show that the observed LAI for potato can be identified as the best indicator for the crop height. Model 7 (EVI2, row crops) is a better indicator of potato crop height than EVI2 itself. As for wheat, crop height is better correlated to the measured LAI and LAI from Model 9 (EVI2, Wheat) than EVI2. The same results were seen for both Tobacco and Cannabis, Model 10 (SeLI, overall crops) was a better indicator of crop height than SeLI. The observed LAI was the best indicant of the measured above-ground and fresh weight of the potato crop. Model 7 and Model 10 had a better correlation with the above-ground fresh and dry weight, than EVI2 and SeLI, respectively (Fig. 11).

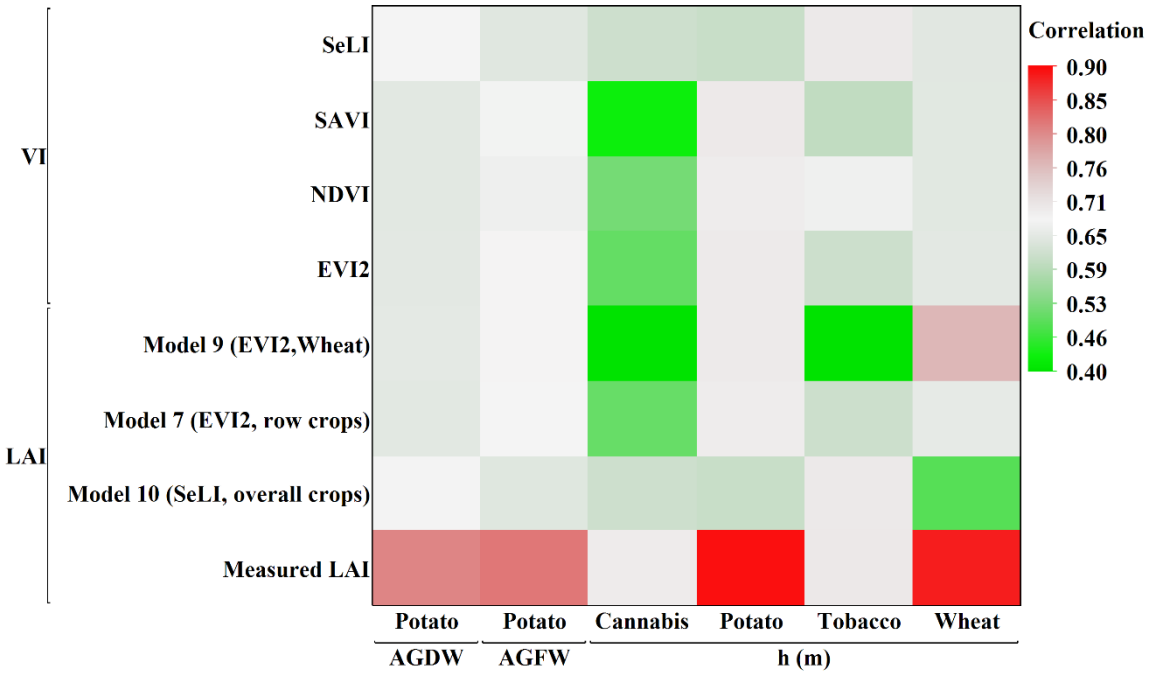

Fig 8. A Correlation heat map between LAI and VI and the plant growth variables

We here proceed to report on the relationships that are most significant for each crop group. Leaf area index can be generated from various vegetation parameters such as the plant height. LAI vs. height relationships are unique to specific crop types due to the vast diversity of canopy structure among crop types. However, simple LAI-height based functions are possible for most of the agricultural types of crops. The major limitation encountered here is the diversity of the crop height – LAI equations that exist in literature. Due to the lack of the universal equation of crop height – LAI, we created the equations for each crop under the local conditions. The utility of basing LAI on crop height is that crop height is a relatively easy parameter to obtain or recollect. In this study, a linear regression was conducted to obtain the relationship between the crop height, the measured LAI, and the best performing models for potato, cannabis, and

tobacco. Figs 12, 13, and 14 indicate that an increase in leaf area is associated with an increased height due to leaf extension as the crop develops. Our analysis shows that the relation between the ground measured LAI and the measured height of the potato crop is essentially linear with an R^2 value 0.818 greater than that obtained when regressing the crop height to LAI obtained from Model 7 (EVI2, row crops) (R^2:0.48) (Fig. 12). Similar crop height-LAI linear relationship was obtained for the wheat crop against measured LAI, with a higher R^2 when regressed to the Model 9 (EVI2, Wheat) (Fig.13). Also, A good relationship exists between the measured height and the measured LAI for the cannabis and tobacco crops with R^2: 0.489 and 0.495, and between the modeled LAI (model 10 derived from SeLI) with R^2: 0.384 and 0.494 for both cannabis and tobacco, respectively (Fig. 14).

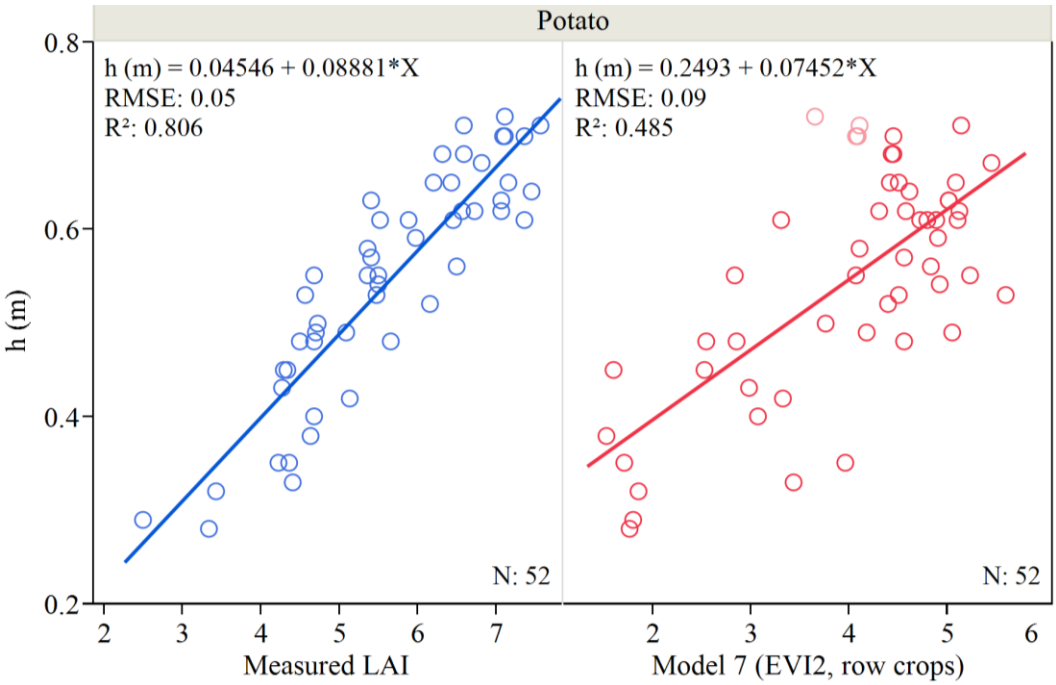

Fig 9. Crop height (h (m)) as a function of Measured LAI (m^2/m^2) and LAI derived from Model 7 (EVI2, row crops) for potato crop studied during the 2019 growing season

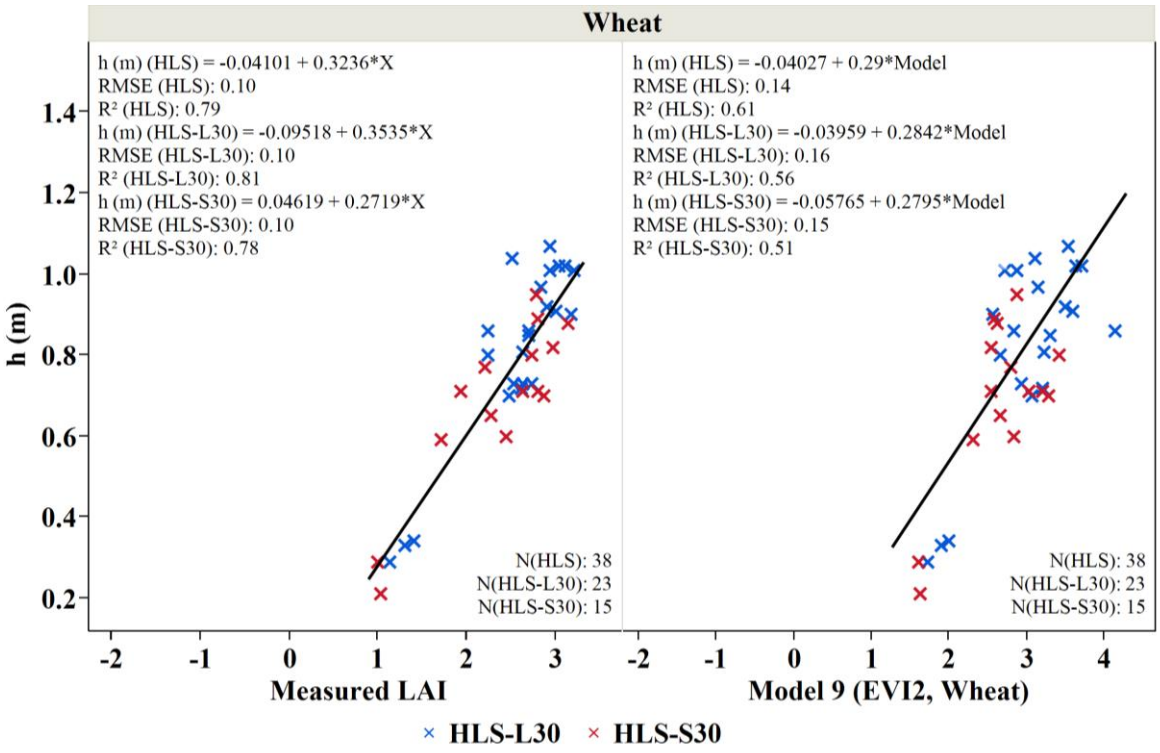

Fig 10. Crop height (h (m)) as a function of Measured LAI (m^2/m^2) for wheat crop studied during the 2019 growing season, separated by satellite, L30 observations in blue and S30 observations in red

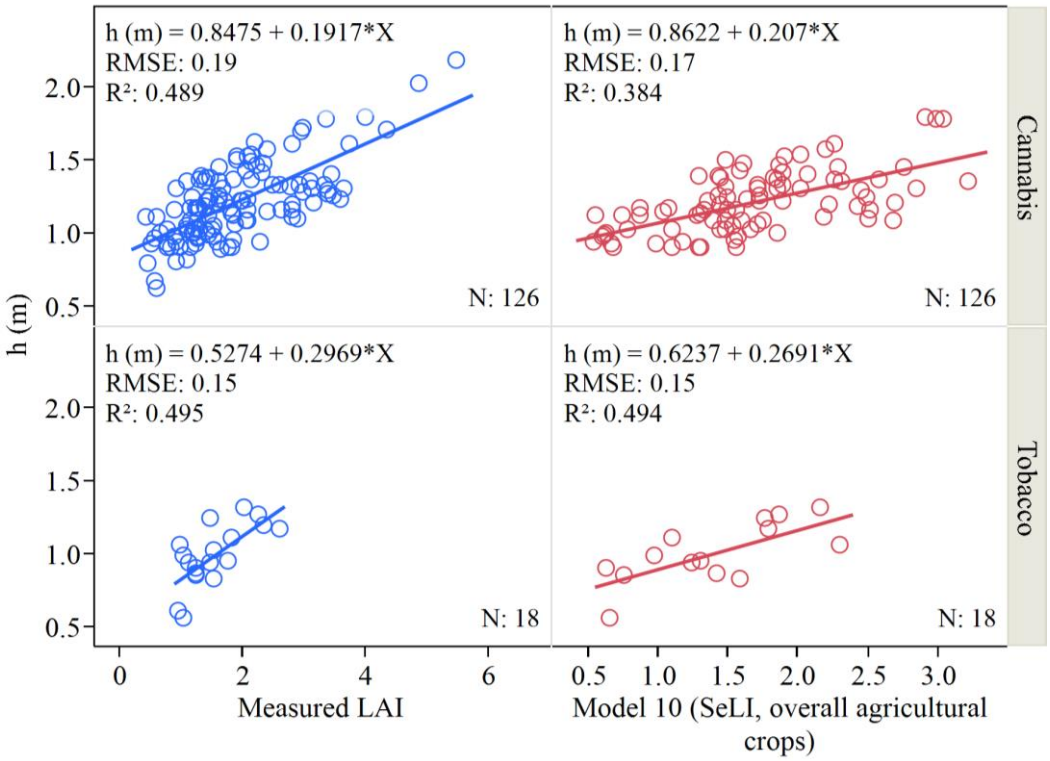

Fig 11. Crop height (h (m)) as a function of measured LAI (m2/m2) and LAI derived from Model 10 (SeLI, overall agricultural crops) for Cannabis and Tobacco crops studied during the 2018 growing season

Above-ground dry and fresh weight of the potato crop studied in 2019 was regressed against the measured LAI, LAI obtained from Model 7 (EVI2, row crops), and the measured height. The relationship between above-ground fresh and dry weights as a function of both the measured LAI and modeled LAI shows that an increase in the leaf area index is associated with an increase in biomass (Fig.14). No saturation in the measurement of biomass from LAI was noticed. The ability of the linear regression to estimate the fresh and dry above-ground biomass of potato from the measured LAI was with a reasonable accuracy level (R^2: app. 0.7) and with a moderate accuracy level (R^2: app. 0.4) for biomass obtained from modeled LAI.

On the other hand, the regression of above-ground dry and fresh biomass of potato against crop height showed that an increase in the above-ground fresh and dry weight of the potato crop is associated with an increase in the crop height (Fig.15). The ability of the linear regression to estimate the fresh and dry above-ground biomass of potato from crop height was with a good accuracy level (R^2: app. 0.6).

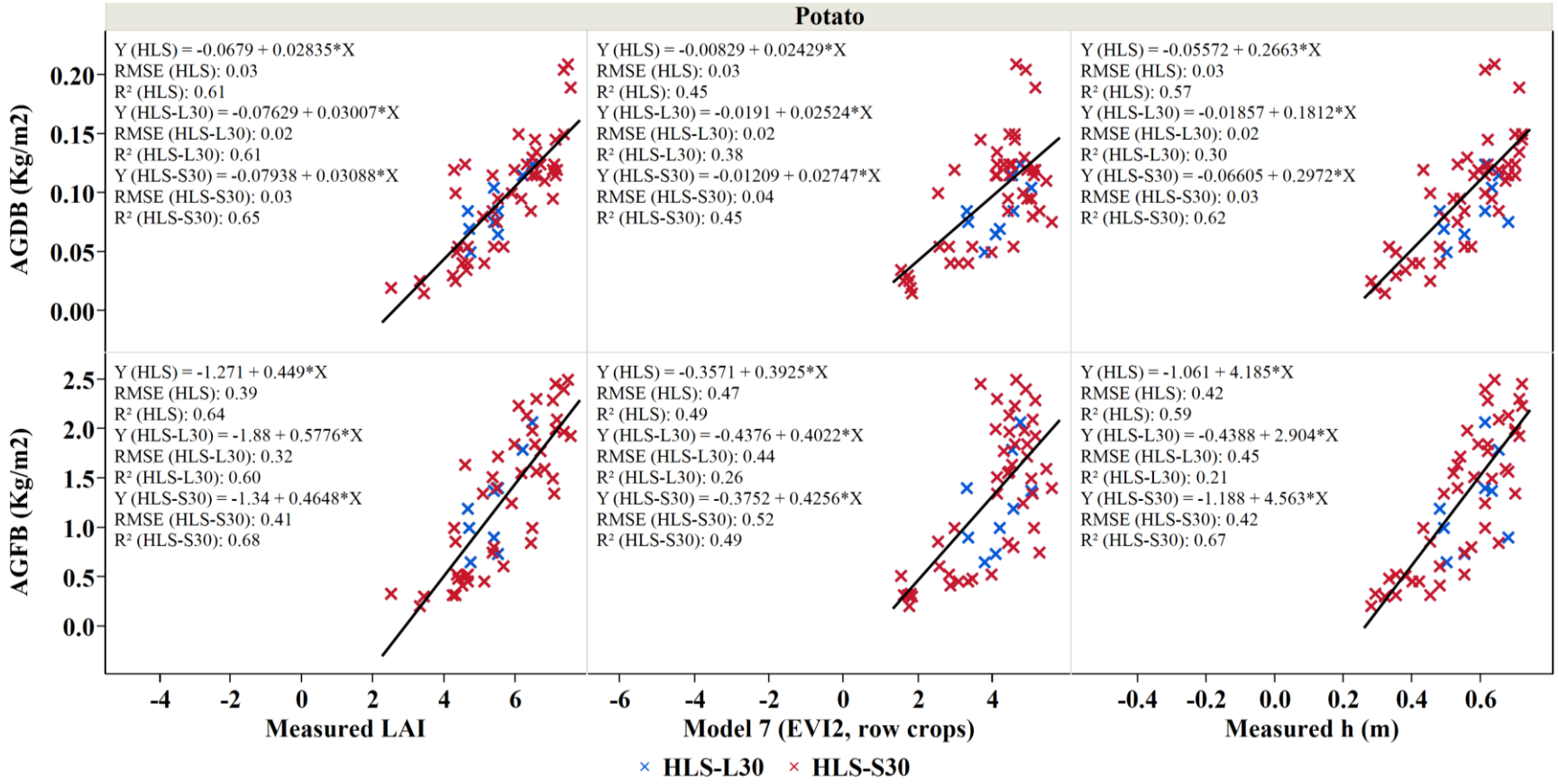

Fig 12. Above-ground fresh and dry weight as a function of LAI derived from Model 7 (EVI2, row crops), Measured LAI, and height (h(m)) for potato fields combined during the 2019 growing season, separated by satellite type, L30 observations in blue, and S30 observations in red

2. Seasonal co-variability in observed and modeled biophysical variables

Potato crop development was monitored regularly during the 2019 growing season, where crop height, LAI, and biomass were measured whereas wheat biophysical parameters measurements were held at the end of the growing season. In this section, we further perform an additional analysis by constructing wheat and potato measured and modeled biophysical parameters (LAI, crop height, and biomass) time-series for the 2019 growing season (Figs 16 and 17). We picked the best relationships for wheat and potato obtained previously in section 3.2, to develop remotely sensed h, LAI, and biomass curves for 2019. For this purpose, we downloaded all L30 and S30 for 2019 during the growing season. The remotely sensed biophysical parameters were derived from EVI2 being reported as the best performing index in this study. The EVI2 evolution of both wheat and potato can be seen in Figs 16 and 17. EVI2 peaks at the mid of season for both wheat and potato then it decreases towards the end of the season.

The phenological differences between both potato and wheat were captured for three potato and wheat farms. Typically, the potato had a higher peak of both modeled and measured LAI during the mid of the growing season, where the average maximum measured LAI for all studied potato fields was found to be 6-8 m^2/m^2 in the mid-season stage (DOY 180). The average minimum measured potato LAI was about 2-3 m^2/m^2 during the beginning of the growing season (DOY 140). Similar modeled LAI evolution was observed for the three potato farms. On the other hand, the measured wheat LAI ranged between 2 and 3 m^2/m^2. Lower wheat LAI values were observed since wheat was monitored during the end of the season, where LAI tends to decrease.

The measured crop height increases as the crop develop. The average minimum measured potato crop height was about 0.4 m during the beginning of the growing season (DOY 140). The maximum average crop height for all studied potato fields was found to be around 0.6 m in the mid-season stage (DOY 180). The measured wheat crop height was found to be approximately 1 m during the end of the season (DOY 135-140). Similar modeled crop height evolution was observed for the three wheat farms.

Similarly, the above-ground fresh and dry biomass increase with crop growth. The aboveground biomass was the lowest during the beginning of the growing season, and it increases to reach its maximum during the mid of the growing season with a value of 2 Kg/m^2 and 0.2 Kg/m^2 for the aboveground fresh and dry biomass, respectively.

Different crop types and their different management practices have given rise to different temporal LAI, crop height, and biomass dynamics. Different observed and measured biophysical variables values of the same crop types but different fields were noticed. These differences can be attributed to the different conditions among the farms within the same crop type due to different agronomic and management practices.

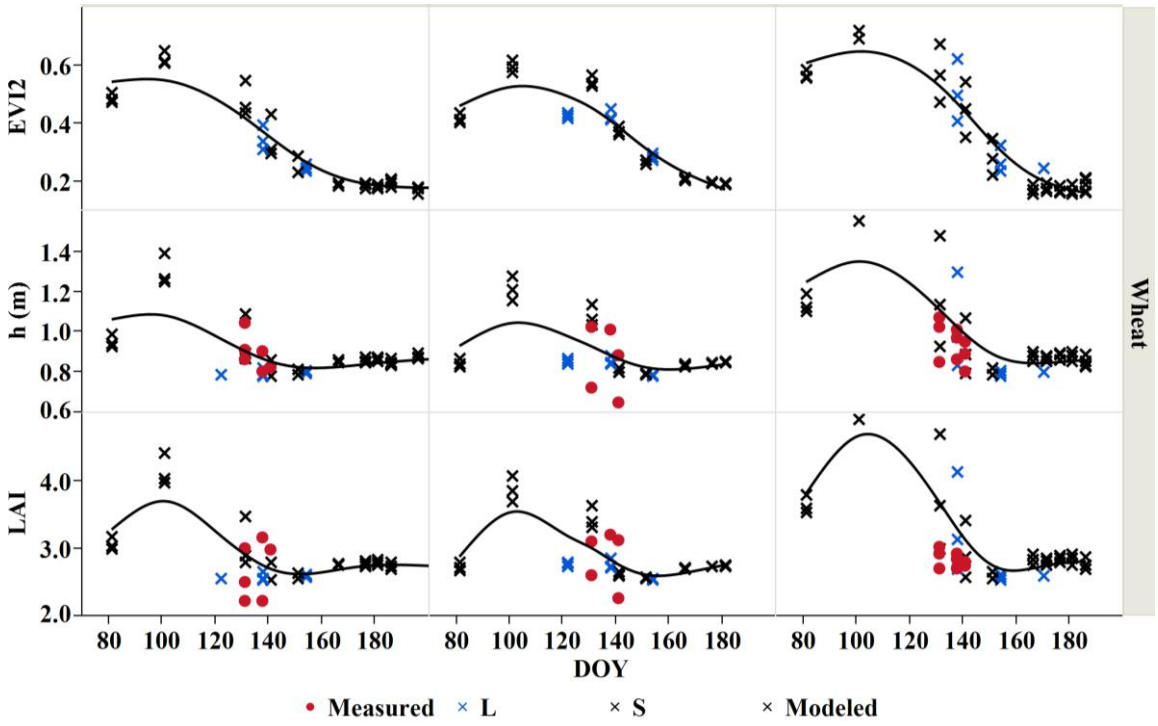

Fig 13. A combined L30–S30 derived and measured biophysical parameters (EVI2, h, and LAI) time-series of wheat for three farms during the 2019 growing season, modeled biophysical parameter and S30 observations in black, measured crop biophysical parameter in red, and L30 observations in blue

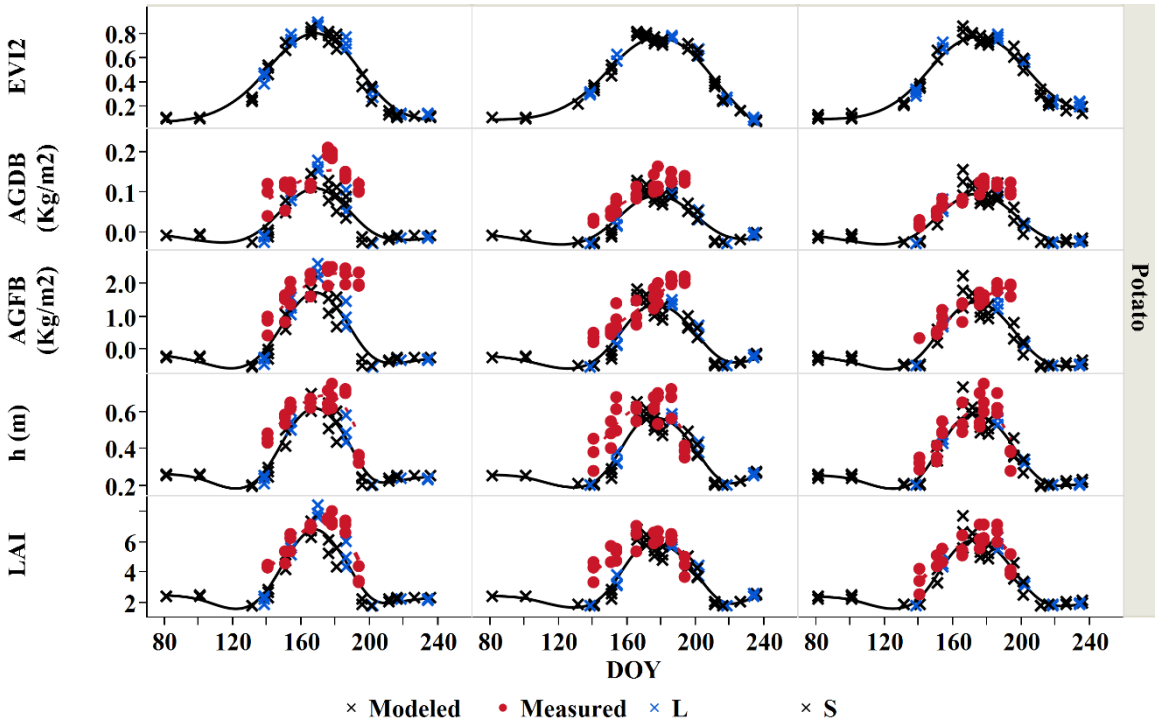

Fig 14. A combined L30–S30 derived and measured biophysical parameters (EVI2, fresh aboveground biomass (AGFB), aboveground dry biomass (AGDB), height (h), and Leaf Area Index (LAI) time-series of potato for three farms during the 2019 growing season, modeled biophysical parameter and S30 observations in black, the measured biophysical parameter in red, and L30 observations in blue

CHAPTER V

DISCUSSION

A. Uncertainties in VI-LAI relationships

To further assess the performance of the studied LAI models against the measured LAI, the measured LAI ranges were arbitrarily divided into the following order: low (0-2 m^2/m^2) (labeled in green, Fig 8&9), medium (2-4 m^2/m^2), and high (>4 m^2/m^2) (labeled in red, Fig 8&9) LAI ranges. Our analysis shows an apparent underestimation of LAI in all tested models for a measured LAI value above 4 m^2/m^2 in all the studied crops, except for tobacco. The underestimation was not noticed in the latter since the measured LAI measurements of tobacco did not exceed 4 m^2/m^2. However, Models 3 and 8 overestimated LAI for potato in the measured LAI range (>4 m^2/m^2).

Uncertainties in LAI-VIs can be grouped into two categories: VIs susceptibility to saturation and errors in LAI observation techniques. LAI models existing in literature are derived from vegetation indices (VIs), which have shown to have little sensitivity to high LAI values, resulting in severe saturation issues. This shows that LAI values that are greater than 4 m^2/m^2 are beyond the prediction power of the studied vegetation indices (Liu et al. 2012; Nguy-Robertson et al. 2014; Viña et al. 2011a). Saturation problems were also identified in all indices when defining the empirical LAI-VI relationship, specifically in tobacco and grains crop groups. Thus, issues with VIs saturation over dense canopies remain a thoughtful challenge (Huete et al. 2002; Kang et al. 2016)

Regarding errors in the LAI measurement method, the underestimation of LAI in the high range of measured LAI can be attributed to the SS1 limitations under high

vegetation cover (LAI range > 4 m^2/m^{-2}). SS1 does not correct for canopy clumping effects; thus, underestimation appears (Jones 2013). Generally, when the canopy is clumped, the leaves hide each other, leaving a gap in between, and thus allowing for more light to reach the ground as compared to randomly distributed leaves. Therefore, the LAI that is calculated using the light transmission theory, such as the SS1 method, becomes underestimated. The underestimation of LAI with SS1 was also observed in previous studies due to the lack of clumping correction (Gower et al. 1999; Wilhelm et al. 2000). Another type of error that falls in the second uncertainty category is that the leaf angle distribution (ELADP) is a fixed constant that is pre-defined by the user according to the crop. However, the chosen ELADP values may not be accurate all over the growing season since the canopy leaves change throughout the entire season (Fang 2015). Moreover, row spacing, crop height, and time of measurement can affect the LAI values.

Based on the produced results, a shift towards improved hemispherical LAI estimation techniques that can provide information on the canopy clumping and leaf angle inclination, measure the LAI at different heights and differentiate between leaves and woody parts through the integration of the infrared techniques is recommended (Jonckheere et al. 2004; Schaefer et al. 2015). As Well, the use of other vegetation indices to improve the saturation problems is yet to be tested.

B. The utility of multi-satellite surface reflectance time-series for monitoring crops in the Bekaa Valley

Multi-satellite data normalization is crucial, and this was addressed through crop biophysical variables time-series generated for monitoring wheat and potato crops in the Bekaa Valley. Time series of crop growth parameters is essential for detecting changes in crop cover, and the combination of data from different ongoing satellite missions provides this opportunity. This study confirms the limited ability of the L30 as a single sensor to capture the full time-series at the farm level. L30 potentially missed biophysical observations at critical growth stages due to its smaller number of images available. Few L30 images were used due to its long revisit time and cloud coverage.

Our results also demonstrate the importance of higher observation frequency achieved with the combination of Landsat-8 and Sentinel-2A satellites comparing to the single use of L30 in crop monitoring. Therefore, LAI and other crop growth variables are appropriately monitored and modeled in this work, especially during fast-developing phenomena, using near-daily and medium resolution (30 m) HLS normalized satellite imageries.

C. Inter-comparison between the evaluated LAI Models

The used HLS VIs Models are very simple to use. Even though these models have shown to be specific to the type of vegetation, site, and sensor (Colombo et al. 2003), our study has shown LAI models: Models 7, 8, and 9 developed initially for row crops, maize, and wheat respectively, were the best performing models for the all crop samples in the study area.

LAI derived from SNAP software performed the poorest among the other LAI Models. LAI retrieval from SNAP is based on neural networks that are trained using radiation transfer models (RTMs). Although the inversion of RTMs proved to be useful

in predicting the LAI biophysical parameter for different types of vegetations (Du et al. 2004; Meroni et al. 2004), however, the inversion of RTMs also has the problem of "ill-posed process" (Combal et al. 2003)which can result in having the similar solution to completely different vegetation structures. To reduce the inaccuracy of the inversion methods, additional information is needed: 1) Ancillary data from another sensor or measured on-site, 2) Canopy architecture, 3) distribution of canopy biophysical variables. The SNAP LAI in this study is underestimated, and this might be since the SNAP biophysical processor lacks the specific ancillary information from which some vegetation architecture features could be derived. The absence of reliable and regularly updated land cover maps at a spatial resolution like that of S2 prevents from tailoring specific algorithms for each of the land cover classes. Consequently, the algorithm may provide reasonably good estimates over all the cases, but undoubtedly unsatisfactory performances as compared to algorithm specific to a given surface type.

CHAPTER VI

CONCLUSION AND RECOMMENDATIONS

In this paper, we focused on the estimation of the Leaf Area Index at a farm level in the Bekaa Valley of Lebanon, using the combined Landsat 8 and Sentinel-2 data at a 30-m spatial resolution. We validated the usefulness of normalizing satellite data in crop leaf area index estimation and empirical LAI based equations determination. Unlike most existing approaches utilizing vegetation indices derived from non-normalized satellite data in order to estimate LAI, we derived the vegetation indices using the red and NIR surface reflectance of the harmonized HLS product. The ground measured leaf area index was regressed against the derived vegetation. The best results were achieved for the EVI2 index exhibiting a quadratic fitting for the combined crops. We also validated LAI models existing in the literature and found that HLS EVI2 based models were the best model for the studied crops combined. This study also shows that LAI derived from the artificial neural network through ESA's SNAP biophysical processor is underestimated.

A shift towards improved hemispherical LAI estimation techniques that can provide information on the canopy clumping and leaf angle inclination, measure the LAI at different heights and differentiate between leaves and woody parts through the integration of the infrared techniques is recommended (Jonckheere et al. 2004; Schaefer et al. 2015). The use of other vegetation indices to improve the saturation problems is yet to be tested.

APPENDIX

Appendix Tables

Table A1. Statistics obtained with linear, polynomial 2nd order logarithmic, square root, and exponential for each of the studied index for the combined crops. The best-fitting is boldfaced.

Index	Linear Fitting			Polynomial Fitting, 2nd order			Logarithmic Fitting			Square root Fitting			Exponential Fitting		
	R^2	RMSE	P-value	R^2	RMSE	P-value	R^2	RMSE	P-value	R^2	RMSE	P-value	R^2	RMSE	P-value
EVI2 (n=432)	0.52	1.06	<0.0001	**0.6**	1.02	<0.0001	0.43	1.16	<0.0001	0.48	1.1	<0.0001	0.54	1.03	<0.001
	6.23EVI2-0.075			5.45EVI2+9.4 (EVI2-0.41)^2-0.06			4.58+2.12log (EVI2)			7.55 Sqrt (EVI2)-2.24			4.01Exp (EVI2)-3.67		
NDVI (n=432)	0.39	1.2	<0.0001	**0.5**	1.15	<0.0001	0.33	1.25	<0.0001	0.36	1.22	<0.0001	0.42	1.17	<0.001
	5.17NDVI-0.45			5.48NDVI+9.86(NDVI-0.56)^2-0.96			3.93+2.29 log (NDVI)			7.07 Sqrt (NDVI)-2.76			3.04Exp (NDVI)-2.96		
SAVI (n=432)	0.48	1.09	<0.0001	**0.5**	1.04	<0.0001	0.4	1.18	<0.0001	0.45	1.13	<0.0001	0.51	1.07	<0.001
	5.17SAVI-0.45			6.3SAVI+13.5(SAVI-0.4)^2-0.38			4.75+2.29 log (SAVI)			8.23 Sqrt (SAVI)-2.63			3.6Exp (SAVI)-4.5		
SeLI (n=315)	0.2	1.1	<0.0001	**0.21**	1.08	<0.0001	0.21	1.09	<0.0001	0.21	1.09	<0.0001	0.19	1.11	<0.001
	3.55SeLI+0.75			3.65SeLI+5.14(SeLI-0.4)2+0.84			3.4+1.24 log (SeLI)			4.39 Sqrt (SeLI)-0.54			2.23 Exp (SeLI)-1.19		

Table A2. Statistics obtained with linear, polynomial 2nd order logarithmic, square root, and exponential for each of the studied index divided by the crop ground and satellite. The best-fitting is boldfaced.

Crop Group	Index	Satellite	Linear Fitting			Polynomial Fitting, 2nd order			Logarithmic Fitting			Square root Fitting			Exponential Fitting		
			R^2	RMSE	P-value	R^2	RMSE	P-value	R^2	RMSE	P-value	R^2	RMSE	P-value	R^2	RMSE	P-value
Wheat & Barley	EVI2	HLS-L30 (n=21)	0.47	0.61	0.0006	**0.76**	0.39	<0.0001	0.66	0.48	<0.0001	0.56	0.55	<0.0001	0.4	0.64	0.0018
			3.7EVI2+0.99			3.3EVI2+19.3 (EVI2-0.4)^2 +1.6			3.96+1.5log (EVI2)			4.9Sqrt (EVI2)-0.56			2.3Exp (EVI2)-0.95		
		HLS-S30 (n=16)	0.35	0.77	0.0157	0.41	0.75	0.03	**0.42**	0.73	<0.0001	0.39	0.74	0.0099	0.32	0.78	0.02
			4.96EVI2-0.33			3.6EVI2+13.6(EVI2-0.4)^2+1.06			3.94+1.7log (EVI2)			5.96 Sqrt (EVI2)-1.4			3.3Exp (EVI2)-2.6		
		Combined (n=37)	0.39	0.67	<0.0001	**0.57**	0.57	<0.0001	0.53	0.59	<0.0001	0.46	0.63	<0.0001	0.36	0.69	<0.0001
			4.03EVI2+0.7			3.3EVI2+16.04(EVI2-0.41)^2+1.36			3.9+1.55log (EVI2)			5.17 Sqrt (EVI2)-0.8			2.5Exp (EVI2)-1.4		
	NDVI	HLS-L30 (n=21)	0.46	0.61	0.0007	**0.73**	0.44	<0.0001	0.61	0.52	<0.0001	0.53	0.57	0.0002	0.3	0.65	0.0022
			2.9NDVI+0.8			2.72NDVI+11.8(NDVI-0.58)^2+1.33			3.55+1.7 log (NDVI)			4.6Sqrt (NDVI)-0.94			1.5Exp (NDVI)-0.23		
		HLS-S30 (n=16)	0.32	0.78	0.02	**0.39**	0.77	0.0422	0.39	0.74	0.01	0.35	0.77	0.0142	0.29	0.8	0.0286
			3.63NDVI+0.29			2.63NDVI+7.64(NDVI-0.57)^2+1.02			3.43+1.77log (NDVI)			5.22 Sqrt (NDVI)-1.54			2.04Exp (NDVI)-1.2		
		Combined (n=37)	0.39	0.67	<0.0001	**0.53**	0.59	<0.0001	0.5	0.614	<0.0001	0.44	0.64	<0.0001	0.34	0.7	0.0001
			3.14NDVI+0.6			2.66NDVI+9.36(NDVI-0.58)^2+1.17			3.49+1.74log (NDVI)			4.8 Sqrt (NDVI)-1.15			1.66Exp (NDVI)-0.5		
	SAVI	HLS-L30 (n=21)	0.49	0.59	0.0004	**0.8**	0.37	<0.001	0.67	0.48	<0.001	0.58	0.54	<0.001	0.43	0.62	0.0011
			4.16SAVI+0.8			3.4SAVI+22.8(SAVI-0.4)^2+1.5			4.1+1.66 log (SAVI)			5.41Sqrt (SAVI)-0.89			2.62Exp (SAVI)-1.48		
		HLS-S30 (n=16)	0.32	0.76	0.0135	**0.42**	0.75	<0.0001	0.42	0.72	0.0065	0.39	0.74	0.009	0.34	0.78	0.0177
			5.44SAVI+0.11			3.82SAVI+14.77(SAVI-0.4)^2+0.95			4.07+1.81 log (SAVI)			6.48 Sqrt (SAVI)-1.79			3.64Exp (SAVI)-3.14		

Crop Group	Index	Satellite	Linear Fitting			Polynomial Fitting, 2nd order			Logarithmic Fitting			Square root Fitting			Exponential Fitting		
			R^2	RMSE	P-value	R^2	RMSE	P-value	R^2	RMSE	P-value	R^2	RMSE	P-value	R^2	RMSE	P-value
Vegetables	SeLI	Combined (n=37)	0.41	0.66	<0.0001	**0.58**	0.56	<0.0001	0.53	0.59	<0.0001	0.48	0.62	<0.0001	0.37	0.68	<0.0001
			4.5SAVI+0.6			3.44SAVI+18.66(SAVI-0.4)^2+1.3			4.06+1.69log (SAVI)			5.7 Sqrt (SAVI)-1.15			2.9Exp (SAVI)-1.9		
		S-2 (n=18)	0.44	0.85	0.0026	**0.55**	0.78	0.0023	0.54	0.77	0.0005	0.49	0.81	0.001	0.4	0.88	0.0045
			4.52SeLI+0.33			4.27SeLI+13.74(SeLI-0.4)^2+0.75			3.8+1.66 log (SeLI)			5.67 Sqrt (SeLI)-1.36			2.88Exp (SeLI)-2.21		
	EVI2	HLS-L30 (n=20)	0.72	0.61	<0.0001	**0.8**	0.53	<0.0001	0.55	0.77	0.0002	0.64	0.69	<0.0001	0.76	0.56	<0.0001
			6.48EVI2-0.23			4.82EVI2+10.6 (EVI2-0.27)^2-5.9e-5			3.79+1.57log (EVI2)			6.7Sqrt (EVI2)-1.85			4.6Exp (EVI2)-4.57		
		HLS-S30 (n=54)	0.13	0.902	0.0065	**0.23**	0.85	<0.0001	0.18	0.87	0.0015	0.15	0.89	0.003	0.11	0.91	0.0124
			2.45EVI2+1.27			1.72EVI2+13.57 (EVI2-0.427)^2+1.86			3.22+0.97log (EVI2)			3.204 Sqrt (EVI2) +0.26			1.5Exp (EVI2) +0.0009		
		Combined (n=74)	0.33	0.87	<0.0001	**0.36**	0.85	<0.0001	0.35	0.85	<0.0001	0.35	0.86	<0.0001	0.31	0.88	<0.0001
			3.85EVI2+0.63			3.77EVI2+6.9 (EVI2-0.38)^2+0.83			3.46+1.26log (EVI2)			4.59 Sqrt (EVI2)-0.66			2.5Exp (EVI2)-1.65		
	NDVI	HLS-L30 (n=20)	0.63	0.73	<0.0001	**0.73**	0.63	<0.0001	0.5	0.85	0.0009	0.57	0.79	0.0003	0.68	0.68	<0.0001
			5.53NDVI-0.76			4.8NDVI+10.4(NDVI-0.43)^2-0.75			3.43+1.97 log (NDVI)			6.8Sqrt (NDVI)-2.76			3.54Exp (NDVI)-3.19		
		HLS-S30 (n=54)	0.12	0.9	0.0089	**0.17**	0.89	0.0077	0.15	0.89	0.0041	0.14	0.9	0.0058	0.11	0.91	0.0147
			2NDVI-1.1			1.26NDVI+6.9(NDVI-0.59)^2+0.76			2.93+1.06log (NDVI)			2.99 Sqrt (NDVI)-0.04			1.07Exp (NDVI)-0.34		
		Combined (n=74)	0.28	0.899	<0.0001	**0.3**	0.895	<0.0001	0.29	0.89	<0.0001	0.29	0.89	<0.0001	0.26	0.9	<0.0001
			3.07NDVI+0.44			2.8NDVI+3.96(NDVI-0.55)^2+0.717			3.1+1.45log (NDVI)			4.34Sqrt (NDVI)-1.03			1.74Exp (NDVI)-0.93		
	SAVI	HLS-L30 (n=20)	0.69	0.64	<0.0001	**0.797**	0.54	<0.0001	0.53	0.79	0.0002	0.61	0.72	<0.0001	0.74	0.59	<0.0001
			6.9SAVI-0.3			5.21SAVI+5.2(SAVI-028)^2-0.177			3.88+1.67 log (SAVI)			7.08Sqrt (SAVI)-2.09			5.03Exp (SAVI)-5.16		
		HLS-S30	0.1	0.9	0.0177	**0.216**	0.867	0.002	0.144	0.9	0.0046	0.12	0.91	0.0089	0.08	0.92	0.0291

Crop Group	Index	Satellite	Linear Fitting			Polynomial Fitting, 2nd order			Logarithmic Fitting			Square root Fitting			Exponential Fitting		
			R^2	RMSE	P-value	R^2	RMSE	P-value	R^2	RMSE	P-value	R^2	RMSE	P-value	R^2	RMSE	P-value
		(n=54)	2.38SAVI-1.32			1.2SAVI-17.64(SAVI-0.41)^2+2.1			3.2+0.95 log (SAVI)			3.11Sqrt (SAVI)+0.336			1.48Exp (SAVI)+0.052		
		Combined (n=74)	0.3	0.89	<0.0001	**0.33**	0.87	<0.0001	0.32	0.876	<0.0001	31	0.88	<0.0001	0.285	0.9	<0.0001
			4.02SAVI-0.58			3.76SAVI-8.9(SAVI-0.38)^2+0.86			3.5+1.32 log (SAVI)			4.76Sqrt (SAVI)-0.764			2.68Exp (SAVI)-1.86		
	SeLI	S-2 (n=72)	0.27	0.93	<0.0001	**0.32**	0.89	<0.0001	0.31	0.9	<0.0001	0.29	0.91	<0.0001	**0.3**	0.96	<0.0001
			2.96SeLI+0.77			3.14SeLI+6.03(SeLI-0.43)^2+0.91			3.15+1.14log (SeLI)			3.89 Sqrt (SeLI)-0.43			1.72 Exp (SeLI)-0.63		
Cannabis	EVI2	HLS-L30 (n=40)	0.28	0.69	0.0003	**0.3**	0.68	0.0008	0.25	0.71	0.001	0.27	0.7	0.0006	0.29	0.68	0.0003
			5.76EVI2-0.06			5.88EVI2+19.5 (EVI2-0.56)^2-0.2			3.24+1.29log (EVI2)			5.58Sqrt (EVI2)-1.37			4.46Exp (EVI2)-4.37		
		HLS-S30 (n=96)	0.31	0.69	<0.0001	**0.34**	0.68	<0.0001	0.26	0.72	<0.001	0.3	0.7	<0.0001	0.32	0.689	<0.001
			5.11EVI2+0.46			4.73EVI2+11.8 (EVI2-0.28)^2+0.47			3.57+1.26log (EVI2)			5.2 Sqrt (EVI2)-0.82			3.81Exp (EVI2)-3.17		
		Combined (n=136)	0.31	0.7	<0.001	**0.33**	0.69	<0.0001	0.26	0.73	<0.0001	0.29	0.72	<0.0001	0.32	0.7	<0.0001
			5.4EVI2+0.27			5.05EVI2+13.06 (EVI2-0.28)^2+0.27			3.52+1.3log (EVI2)			5.4 Sqrt (EVI2)-1.05			4.07Exp (EVI2)-3.61		
	NDVI	HLS-L30 (n=40)	0.22	0.72	0.0019	**0.23**	0.72	0.0065	0.2	0.73	0.0034	0.217	0.72	0.0024	0.23	0.72	0.0016
			3.363NDVI-0.04			3.86NDVI+6.68(NDVI-0.42)^2-0.2			2.65+1.29log (NDVI)			4.4Sqrt (NDVI)-1.34			2.43Exp (NDVI)-2.24		
		HLS-S30 (n=96)	0.27	0.71	<0.0001	**0.3**	0.7	<0.0001	0.22	0.74	<0.0001	0.25	0.72	<0.0001	0.28	0.71	<0.0001
			3.22NDVI-0.51			3.29NDVI+6.86(NDVI-0.43)^2+0.35			2.92+1.13log (NDVI)			3.91 Sqrt (NDVI)-0.62			2.11Exp (NDVI)-1.38		
		Combined (n=136)	0.25	0.73	<0.0001	**0.29**	0.72	<0.0001	0.211	0.75	<0.0001	0.23	0.75	<0.0001	0.27	0.72	<0.0001
			3.38NDVI+0.33			3.47NDVI+7.79(NDVI-0.43)^2+0.16			2.84+1.18log (NDVI)			4.09Sqrt (NDVI)-0.86			2.24Exp (NDVI)-1.68		
	SAVI	HLS-L30 (n=40)	0.28	0.69	0.0004	**0.31**	0.69	0.001	0.24	0.71	0.0012	0.26	0.7	0.0007	0.29	0.69	0.0003
			5.9SAVI-0.15			6.19SAVI+21.25(SAVI-0.27)^2-0.3			3.29+1.37 log (SAVI)			5.8Sqrt (SAVI)-1.54			3.84Exp (SAVI)-3.66		

Crop Group	Index	Satellite	Linear Fitting			Polynomial Fitting, 2nd order			Logarithmic Fitting			Square root Fitting			Exponential Fitting		
			R^2	RMSE	P-value	R^2	RMSE	P-value	R^2	RMSE	P-value	R^2	RMSE	P-value	R^2	RMSE	P-value
		HLS-S30 (n=96)	0.2	0.75	<0.0001	**0.2**	0.75	<0.0001	0.19	0.759	<0.0001	0.2	0.75	<0.0001	0.2	0.75	<0.0001
			4.717SAVI+0.56			4.74SAVI+4.88(SAVI-0.288)^2+0.52			3.44+1.17 log (SAVI)			4.8Sqrt (SAVI)-0.62			3.54Exp (SAVI)-2.8		
		Combined (n=136)	0.22	0.45	<0.0001	**0.22**	0.75	<0.0001	0.19	0.76	<0.0001	0.21	0.75	<0.0001	0.22	0.75	<0.0001
			5.15SAVI+0.32			5.21SAVI+9.33(SAVI-0.228)^2+0.25			3.43+1.26 log (SAVI)			5.19Sqrt (SAVI)-0.95			3.9Exp (SAVI)-3.4		
	SeLI	S-2 (n=121)	0.33	0.72	<0.0001	**0.34**	0.72	<0.0001	0.29	0.74	<0.0001	0.31	0.73	<0.0001	**0.34**	0.72	<0.0001
			4.2SeLI+0.5			3.65SeLI+5.14(SeLI-0.4)^2+0.84			3.29+1.16 log (SeLI)			4.58 Sqrt (SeLI)-0.67			3.03 Exp (SeLI)-2.33		
Tobacco	EVI2	HLS-L30 (n=9)	0.59	0.51	0.0154	**0.77**	0.41	0.011	0.7	0.43	0.0046	0.65	0.47	0.0084	0.55	0.54	0.0228
			4.12EVI2-0.36			7.07EVI2+16.9(EVI2-0.308)^2-0.24			3.6+1.57log (EVI2)			5.22Sqrt (EVI2)-1.2			2.64Exp (EVI2)-1.99		
		HLS-S30 (n=16)	0.3	0.34	0.0235	**0.32**	0.36	0.08	0.32	0.34	0.02	0.318	1.35	0.0229	0.31	0.34	0.0236
			3.08EVI2+0.91			3.09EVI2+0.59 (EVI2-0.22)^2+0.911			2.606+0.647log (EVI2)			2.87 Sqrt (EVI2)+0.25			2.43Exp (EVI2)-1.45		
		Combined (n=25)	0.43	0.42	0.0004	**0.44**	0.42	0.0015	0.42	0.72	0.0004	0.43	0.41	0.0003	0.41	0.42	0.0005
			3.2EVI2+0.78			3.8EVI2+3.17 (EVI2-0.25)^2+0.68			2.9+0.89log (EVI2)			3.57Sqrt (EVI2)-0.15			2.25Exp (EVI2)-1.3		
	NDVI	HLS-L30 (n=9)	0.67	0.46	0.007	**0.78**	0.41	0.0114	0.74	0.4	0.0028	0.71	0.43	0.0043	0.62	0.56	0.0115
			3.5NDVI-0.12			4.88NDVI+8.48(NDVI-0.433)^2-24			3.18+1.71log (NDVI)			5Sqrt (NDVI)-1.6			1.99Exp (NDVI)-1.48		
		HLS-S30 (n=16)	0.35	0.33	0.015	**0.36**	0.35	0.0552	0.4	0.35	0.0951	0.36	0.34	0.0139	0.34	0.34	0.016
			2.22NDVI+0.831			2.27NDVI+2.39(NDVI-0.34)^2+0.84			2.4+0.722log (NDVI)			2.58 Sqrt (NDVI)+0.1			1.54Exp (NDVI)-0.59		
		Combined (n=25)	0.49	0.39	<0.0001	**0.5**	0.4	0.0005	0.48	0.39	0.0001	0.49	0.39	<0.0001	0.48	0.4	0.0001
			2.7NDVI+0.5			2.9NDVI+1.23(NDVI-0.37)^2+0.5			2.6+1.03log (NDVI)			3.46 Sqrt (NDVI)-0.47			1.67Exp (NDVI)-0.85		
	SAVI	HLS-L30	0.62	0.49	0.0123	**0.77**	0.41	0.0118	0.71	0.43	0.0042	0.66	0.46	0.0071	0.57	0.52	0.0178

Crop Group	Index	Satellite	Linear Fitting			Polynomial Fitting, 2nd order			Logarithmic Fitting			Square root Fitting			Exponential Fitting		
			R^2	RMSE	P-value	R^2	RMSE	P-value	R^2	RMSE	P-value	R^2	RMSE	P-value	R^2	RMSE	P-value
		(n=9)	4.65SAVI-0.19			7.3SAVI+18.9(SAVI-0.311)^2-0.38			3.7+1.72 log (SAVI)			5.7Sqrt (SAVI)-1.5			3.04Exp (SAVI)-2.55		
		HLS-S30 (n=16)	0.18	0.38	0.106	**0.19**	0.39	0.002	0.19	0.377	0.083	0.19	0.38	0.093	0.16	0.38	0.114
			1.81SAVI+1.12			1.93SAVI-6.69(SAVI-0.25)^2+1.14			2.24+0.46 log (SAVI)			1.87Sqrt (SAVI)+0.65			1.36Exp (SAVI)-0.179		
		Combined (n=25)	0.37	0.43	0.0012	**0.37**	0.45	0.0057	0.35	0.44	0.0017	0.369	0.44	0.0013	0.369	0.44	0.0013
			3.08SAVI+0.75			3.13SAVI-0.58(SAVI-0.276)^2+0.74			2.73+0.82 log (SAVI)			3.3Sqrt (SAVI)-0.099			2.19Exp (SAVI)-1.3		
	SeLI	S-2 (n=19)	0.16	0.466	0.0837	**0.18**	0.47	0.2022	0.14	0.47	0.1164	0.15	0.46	0.09	0.17	0.46	0.0793
			2.25SeLI+1.11			2.12SeLI+7.26(SeLI-0.24)^2+1.09			2.35+0.46 log (SeLI)			2.09 Sqrt (SeLI)+0.65			1.76 Exp (SeLI)-0.59		
Potato	EVI2	HLS-L30 (n=55)	0.4	1.2	<0.0001	**0.5**	1.144	<0.0001	0.34	1.3	<0.0001	0.37	1.2	<0.0001	0.43	1.2	<0.0001
			6.47EVI2-0.86			7.07EVI2+20.8(EVI2-0.51)^2-1.66			4.41+2.71log (EVI2)			8.53Sqrt (EVI2)-3.5			4.01Exp (EVI2)-4.33		
		HLS-S30 (n=105)	0.56	1.34	<0.0001	**0.6**	1.27	<0.0001	0.49	1.43	<0.0001	0.53	1.37	<0.0001	0.58	1.3	<0.0001
			9.17EVI2-1.39			9.19EVI2+15.25 (EVI2-0.55)^2-1.8			6.48+4.36log (EVI2)			12.9 Sqrt (EVI2)-5.82			5.29Exp (EVI2)-5.644		
		Combined (n=160)	0.5	1.37	<0.0001	**0.56**	1.28	<0.0001	0.43	1.47	<0.0001	0.47	1.42	<0.0001	0.53	1.33	<0.0001
			8.64EVI2-1.4			8.77EVI2+18.08 (EVI2-0.54)^2-1.9			5.88+3.933log (EVI2)			11.9 Sqrt (EVI2)-5.37			5.11Exp (EVI2)-5.6		
	NDVI	HLS-L30 (n=55)	0.28	1.35	<0.0001	**0.4**	1.25	<0.0001	0.24	1.38	0.0001	0.26	1.36	<0.001	0.31	1.32	<0.0001
			6.2NDVI-1.7			9.25NDVI+29.6(NDVI-0.67)^2-4.33			3.88+3.43log (NDVI)			9.32Sqrt (NDVI)-5.16			3.42Exp (NDVI)-4.33		
		HLS-S30 (n=105)	0.38	1.57	<0.0001	**0.49**	1.43	<0.0001	0.32	1.66	<0.0001	0.36	1.6	<0.0001	0.42	1.53	<0.0001
			9.7NDVI-3.15			12.88NDVI+31.87(NDVI-0.708)^2-5.9			5.7+5.58log (NDVI)			14.9 Sqrt (NDVI)-8.78			3.84Exp (NDVI)-3.66		
		Combined (n=160)	0.35	1.57	<0.0001	**0.46**	1.44	<0.0001	0.29	1.64	<0.0001	0.32	1.6	<0.0001	0.37	1.54	<0.0001
			8.82NDVI-2.87			12.16NDVI+32.67(NDVI-0.69)^2-5.7			5.19+5.0058log (NDVI)			13.45Sqrt (NDVI)-7.8			4.7Exp (NDVI)-6.3		

Crop Group	Index	Satellite	Linear Fitting			Polynomial Fitting, 2nd order			Logarithmic Fitting			Square root Fitting			Exponential Fitting		
			R^2	RMSE	P-value	R^2	RMSE	P-value	R^2	RMSE	P-value	R^2	RMSE	P-value	R^2	RMSE	P-value
	SAVI	HLS-L30 (n=55)	0.4	1.23	<0.0001	**0.5**	1.13	<0.0001	0.34	1.29	<0.0001	0.37	1.26	<0.0001	0.42	1.21	<0.0001
			7.5SAVI-1.2			8.65SAVI+29.92(SAVI-0.48)^2-2.29			4.76+3.04 log (SAVI)			9.68Sqrt (SAVI)-4.2			4.78Exp (SAVI)-5.4		
		HLS-S30 (n=105)	0.54	1.35	<0.0001	**0.59**	1.2	<0.0001	0.47	1.45	<0.0001	0.51	1.4	<0.0001	0.56	1.32	<0.0001
			11.05SAVI-2.13			11.57SAVI+24.7(SAVI-0.52)^2-2.8			7.07+4.99 log (SAVI)			15.13Sqrt (SAVI)-7.19			6.65Exp (SAVI)-7.67		
		Combined (n=160)	0.49	1.39	<0.0001	**0.56**	1.28	<0.0001	0.42	1.48	<0.0001	0.46	1.43	<0.0001	0.52	1.35	<0.0001
			10.27SAVI-2.009			11SAVI+27.6(SAVI-0.52)^2-2.87			6.4+4.45 log (SAVI)			13.7Sqrt (SAVI)-6.49			6.3Exp (SAVI)-7.3		
	SeLI	S-2 (n=85)	0.02	1.66	0.194	**0.02**	1.66	0.36	0.023	1.65	0.162	0.02	1.65	0.1776	0.01	1.66	0.2089
			2.28SeLI+1.6			1.92SeLI+7.02(SeLI-0.5)^2+1.86			3.5+1.2107 log (SeLI)			3.22 Sqrt (SeLI)+0.477			1.35 Exp (SeLI)+0.5		

BIBLIOGRAPHY

Anderson, M., Neale, C., Li, F., Norman, J., Kustas, W., Jayanthi, H., & Chavez, J. (2004). Upscaling ground observations of vegetation water content, canopy height, and leaf area index during SMEX02 using aircraft and Landsat imagery. *Remote Sensing of Environment, 92*, 447-464

Ariza-Carricondo, C., Di Mauro, F., de Beeck, M.O., Roland, M., Gielen, B., Vitale, D., Ceulemans, R., & Papale, D. (2019). A comparison of different methods for assessing leaf area index in four canopy types. *Central European Forestry Journal, 65*, 67-80

Asner et al. (2003). Global synthesis of leaf area index observations: implications for ecological and remote sensing studies. *Global Ecology and Biogeography, 12*, 191-205

Baghzouz, M., Devitt, D.A., Fenstermaker, L.F., & Young, M.H. (2010). Monitoring vegetation phenological cycles in two different semi-arid environmental settings using a ground-based NDVI system: A potential approach to improve satellite data interpretation. *Remote Sensing, 2*, 990-1013

Baret, F., & Guyot, G. (199 .(1Potentials and limits of vegetation indices for LAI and APAR assessment. *Remote Sensing of Environment, 35*, 161-173

Barsi, J.A., Alhammoud, B., Czapla-Myers, J., Gascon, F., Haque, M.O., Kaewmanee, M., Leigh, L., & Markham, B.L. (2018). Sentinel-2A MSI and Landsat-8 OLI radiometric cross-comparison over desert sites. *European Journal of Remote Sensing, 51*, 822-837

Behnia, P. (2005). Comparison between four methods for data fusion of ETM+ multispectral and pan images. *Geo-Spatial Information Science, 8*103-98 ,
Bochenek, Z., Dąbrowska-Zielińska, K., Gurdak, R., Niro, F., Bartold, M.

Grzybowski, P. (2017). Validation of the LAI biophysical product derived from Sentinel-2 and Proba-V images for winter wheat in western Poland. *Geoinformation Issues, 9*26--15 ,

Boegh, E., Søgaard, H., Broge, N., Hasager, C., Jensen, N., Schelde, K., & Thomsen, A. (2002). Airborne multispectral data for quantifying leaf area index, nitrogen concentration, and photosynthetic efficiency in agriculture. *Remote Sensing of Environment, 81*, 179-193

Boschetti, L., Roy, D.P., Justice, C.O., & Humber, M.L. (2015). MODIS–Landsat fusion for large area 30 m burned area mapping. *Remote Sensing of Environment, 161*, 27-42

Breda, N.J. (2003). Ground-based measurements of leaf area index :a review of methods, instruments and current controversies. *Journal of experimental botany, 54*, 2403-2417

Broge, N.H., & Leblanc, E. (2001). Comparing prediction power and stability of broadband and hyperspectral vegetation indices for estimation of green leaf area index and canopy chlorophyll density. *Remote Sensing of Environment, 76*, 156-172

Campbell, G., & Van Evert, F. (1994). Light interception by plant canopies: efficiency and architecture. *Resource capture by crops*, 35-52

Campbell, G.S. (1986). Extinction coefficients for radiation in plant canopies calculated using an ellipsoidal inclination angle distribution. *Agricultural and forest meteorology, 36*, 317-321

Campos-Taberner, M., García-Haro, F.J., Camps-Valls, G., Grau-Muedra, G., Nutini, F., Crema, A., & Boschetti, M. (2016). Multitemporal and multiresolution leaf area index retrieval for operational local rice crop monitoring. *Remote Sensing of Environment, 187*, 102-118

Casa et al. (2019). Measurement and estimation of leaf area index (LAI) using commercial instruments and smartphone-based systems. In, *IOP Conference Series: Earth and Environmental Science* (p. 012006): IOP Publishing

Charbonnier, F. (2013). Measuring and modeling light, water and carbon budgets and net primary productivity in a coffee-based agroforestry system of Costa Rica. In: Université de Lorraine

Chen et al. (1992). Defining leaf area index for non-flat leaves. *Plant, Cell & Environment, 15*, 421-429

Claverie et al. (2018). The Harmonized Landsat and Sentinel-2 surface reflectance data set. *Remote Sensing of Environment, 219*, 145-161

Claverie, M., Demarez, V., Duchemin, B., Hagolle, O., Ducrot, D., Marais-Sicre, C., Dejoux, J.-F., Huc, M., Keravec, P., & Béziat, P. (2012). Maize and sunflower biomass estimation in southwest France using high spatial and temporal resolution remote sensing data. *Remote Sensing of Environment, 124*, 844-857

Colombo, R., Bellingeri, D., Fasolini, D., & Marino, C.M. (2003). Retrieval of leaf area index in different vegetation types using high resolution satellite data. *Remote Sensing of Environment, 86*, 120-131

Comair, F.G. (1998). *Litani water management: Prospect for the future*. Université saint-esprit de Kaslik

Combal, B., Baret, F., Weiss, M., Trubuil, A., Mace, D., Pragnere, A., Myneni, R ,. Knyazikhin, Y., & Wang, L. (2003). Retrieval of canopy biophysical variables from

bidirectional reflectance: Using prior information to solve the ill-posed inverse problem. *Remote Sensing of Environment, 84*, 1-15

Deering, D.W. (1978). Rangeland reflectance characteristics measured by aircraft and spacecraft sensors. *Ph. D Dissertation. Texas A&M Universtiy*

Dente, L., Satalino, G., Mattia, F., & Rinaldi, M. (2008). Assimilation of leaf area index derived from ASAR and MERIS data into CERES-Wheat model to map wheat yield. *Remote Sensing of Environment, 112*, 1395-1407

Di Bella, C.M., Paruelo, J.M., Becerra, J., Bacour, C., & Baret, F. (2004). Effect of senescent leaves on NDVI-based estimates of f APAR: Experimental and modelling evidences. *International Journal of Remote Sensing, 25*, 5415-5427

Djamai, N., & Fernandes, R. (2018). Comparison of SNAP-derived Sentinel-2A L2A product to ESA product over Europe. *Remote Sensing, 10*, 926

Dong, J., Zhuang, D., Huang, Y., & Fu, J. (2009). Advances in multi-sensor data fusion: Algorithms and applications. *Sensors, 9*, 7771-7784

Du, Y., Chen, L.-F., Yang, L., & Liu, Q. (2004). Inversion and spatial scale effects analysis of leaf area index. In, *IGARSS 2004. 2004 IEEE International Geoscience and Remote Sensing Symposium* (pp. 4474-4476): Ieee

Fang, F. (2015). *The retrieval of leaf inclination angle and leaf area index in maize*. University of Twente Faculty of Geo-Information and Earth Observation (ITC)

Fang, H., Liang, S., Hoogenboom, G., Teasdale, J., & Cavigelli, M .(2008) .Corn-yield estimation through assimilation of remotely sensed data into the CSM-CERES-Maize model. *International Journal of Remote Sensing, 29*, 3011-3032

FAO (2019). In: Land and Water Database

Fassnacht et al. (1997). Estimating the leaf area index of north central Wisconsin forests using the Landsat Thematic Mapper. *Remote Sensing of Environment, 61*, 229-245

Feng et al. (2019). An optimized non-linear vegetation index for estimating leaf area index in winter wheat. *Precision Agriculture*, 1-20

Féret, J.-B., Gitelson, A., Noble, S., & Jacquemoud, S. (2017). PROSPECT-D: Towards modeling leaf optical properties through a complete lifecycle. *Remote Sensing of Environment, 193*, 204-215

Gitelson, A.A., Vina, A., Ciganda, V., Rundquist, D.C., & Arkebauer ,T.J. (2005). Remote estimation of canopy chlorophyll content in crops. *Geophysical Research Letters, 32*

González-Sanpedro, M., Le Toan, T., Moreno, J., Kergoat, L., & Rubio, E. (2008). Seasonal variations of leaf area index of agricultural fields retrieved from Landsat data. *Remote Sensing of Environment, 112*, 810-824

Gower et al. (1999). Direct and indirect estimation of leaf area index, fAPAR, and net primary production of terrestrial ecosystems. *Remote Sensing of Environment, 70*, 29-51

Guyot et al .(1992) .Imaging spectroscopy for vegetation studies. *Imaging spectroscopy: Fundamentals and prospective application, 2*, 145-165

Hansen et al. (2003). Reflectance measurement of canopy biomass and nitrogen status in wheat crops using normalized difference vegetation indices and partial least squares regression. *Remote Sensing of Environment, 86*, 542-553

Hansen, M.C., & Loveland, T.R. (2012). A review of large area monitoring of land cover change using Landsat data. *Remote Sensing of Environment, 122*, 66-74
He, L., Zhang, H.-Y., Zhang, Y.-S., Song, X., Feng, W., Kang, G.-Z., Wang, C.-Y., &

Guo, T.-C. (2016). Estimating canopy leaf nitrogen concentration in winter wheat based on multi-angular hyperspectral remote sensing. *European Journal of Agronomy, 73*, 170185-

Hilker, T., Wulder, M.A., Coops, N.C., Seitz, N., White, J.C., Gao, F., Masek, J.G., & Stenhouse, G. (2009). Generation of dense time series synthetic Landsat data through data blending with MODIS using a spatial and temporal adaptive reflectance fusion model. *Remote Sensing of Environment, 113*, 1988-1999

Huete, A., Didan, K., Miura, T., Rodriguez, E.P., Gao, X., & Ferreira, L.G. (2002). Overview of the radiometric and biophysical performance of the MODIS vegetation indices. *Remote Sensing of Environment, 83*, 195-213

Huete, A., Justice, C., & Leeuwen, W. (1996). MODIS Vegetation Index (MOD13), EOS MODIS Algorithm. *Theoretical basis document, NASA Goddard Space Flight Center, Greenbelt, MD*

Huete, A., Liu, H., Batchily, K., & Van Leeuwen, W. (1997). A comparison of vegetation indices over a global set of TM images for EOS-MODIS. *Remote Sensing of Environment, 59*, 440-451

Huete, A.R. (1988). A soil-adjusted vegetation index (SAVI). *Remote Sensing of Environment, 25*, 295-309

Jaafar, H.H., & Ahmad, F.A .(2020) .Time series trends of Landsat-based ET using automated calibration in METRIC and SEBAL: The Bekaa Valley, Lebanon. *Remote Sensing of Environment, 238*, 111034

Jacquemoud, S., & Baret, F. (1990). PROSPECT: A model of leaf optical properties spectra .*Remote Sensing of Environment, 34*, 75-91

Jarlan, L., Balsamo, G., Lafont, S., Beljaars, A., Calvet, J.-C., & Mougin, E. (2008). Analysis of leaf area index in the ECMWF land surface model and impact on latent heat and carbon fluxes: Application to West Africa. *Journal of Geophysical Research: Atmospheres, 113*

Jiang, Z., Huete, A.R., Didan, K., & Miura, T. (2008). Development of a two-band enhanced vegetation index without a blue band. *Remote Sensing of Environment, 112*, 3833-3845

Jonckheere, I., Fleck, S ,.Nackaerts, K., Muys, B., Coppin, P., Weiss, M., & Baret, F. (2004). Review of methods for in situ leaf area index determination: Part I. Theories, sensors and hemispherical photography. *Agricultural and forest meteorology, 121*, 19-35

Jones, H.G .(2013) .*Plants and microclimate: a quantitative approach to environmental plant physiology*. Cambridge university press

Jung, M., Reichstein, M., Ciais, P., Seneviratne, S.I., Sheffield, J., Goulden, M.L., Bonan, G., Cescatti, A., Chen, J., & De Jeu, R. (2010). Recent decline in the global land evapotranspiration trend due to limited moisture supply. *Nature, 467*, 951

Kang, Y., Özdoğan, M., Zipper, S.C., Román, M.O., Walker, J., Hong, S.Y., Marshall, M., Magliulo, V., Moreno, J., & Alonso, L. (2016). How universal is the relationship between remotely sensed vegetation indices and crop leaf area index? A global assessment. *Remote Sensing, 8*, 597

Lillesand, T.M. (1994). Ralph W. Kiefer. *Remote sensing and image interpretation. 3rd ed. New York: John Wiley*

Liu et al .(2004) .Exploring the relationship between red edge parameters and crop variables for precision agriculture. In, *IGARSS 2004. 2004 IEEE International Geoscience and Remote Sensing Symposium* (pp. 1276-1279): IEEE

Liu, J., Pattey, E., & Jégo, G. (2012). Assessment of vegetation indices for regional crop green LAI estimation from Landsat images over multiple growing seasons. *Remote Sensing of Environment, 123*, 347-358

Ma, J., Zhang, W., Marinoni, A., Gao, L., & Zhang, B. (2018). An improved spatial and temporal reflectance unmixing model to synthesize time series of landsat-like images. *Remote Sensing, 10*, 1388

Meroni, M., Colombo, R., & Panigada, C. (2004). Inversion of a radiative transfer model with hyperspectral observations for LAI mapping in poplar plantations. *Remote Sensing of Environment, 92*, 195-206

MOE (2001). Lebanon State of the Environment Report. In

Myneni et al. (1997). Estimation of global leaf area index and absorbed PAR using radiative transfer models. *IEEE Transactions on Geoscience and remote sensing, 35*, 1380-1393

NASA (2013). Landsat 8 Launch.National Aeronautics and Space Administration.

NASA (2016). *Landsat 7 handbook. National Aeronautics and Space Administration* . Nguy-Robertson, A.L., Peng, Y., Gitelson, A.A., Arkebauer, T.J., Pimstein, A., Herrmann, I., Karnieli, A., Rundquist, D.C., & Bonfil, D.J. (2014). Estimating green LAI in four crops: Potential of determining optimal spectral bands for a universal algorithm. *Agricultural and forest meteorology, 192*, 140-148

Pasqualotto et al. (2019a). Multi-Crop Green LAI Estimation with a New Simple Sentinel-2 LAI Index (SeLI). *Sensors, 19*, 904

Pasqualotto, N., Delegido, J., Van Wittenberghe, S., Rinaldi, M., & Moreno, J. (2019b). Multi-crop green LAI estimation with a new simple Sentinel-2 LAI Index (SeLI). *Sensors, 19*, 904

Potter et al. (1996). SunScan Canopy Analysis System. User Manual. *Delta-T Devices, Cambridge, UK*

Reyes-González, A., Kjaersgaard, J., Trooien, T., Reta-Sánchez, D.G., Sánchez-Duarte, J.I., Preciado-Rangel, P., & Fortis-Hernández, M. (2019). Comparison of Leaf Area Index, Surface Temperature, and Actual Evapotranspiration Estimated Using the METRIC Model and In Situ Measurements. *Sensors, 19*, 1857

Rouse et al. (1974). Monitoring the vernal advancement of natural vegetation. *Final report, NASA/GCSFC, Greenbelt, MD, 6*

Rouse Jr, J., Haas, R., Deering, D., Schell, J., & Harlan, J. (1974). Monitoring the Vernal Advancement and Retrogradation (Green Wave Effect) of Natural Vegetation.[Great Plains Corridor]

Schaefer et al .(2015) .Overview of ground based techniques for estimating LAI. *AusCover Good Practice Guidelines: A technical handbook supporting calibration and validation activities of remotely sensed data product*, 88-118

Sharma, L.K., Bu, H., Denton, A., & Franzen ,D.W. (2015). Active-optical sensors using red NDVI compared to red edge NDVI for prediction of corn grain yield in North Dakota, USA. *Sensors, 15*, 27832-27853

Skakun, S., Vermote, E., Roger, J.-C., & Franch, B. (2017). Combined use of Landsat-8 and Sentinel-2A images for winter crop mapping and winter wheat yield assessment at regional scale. *AIMS geosciences, 3*, 163

Sone et al. (2009). Comparison of three methods for estimating leaf area index of upland rice cultivars. *Crop Science, 49*, 1438-1443

Storey ,J., Roy, D.P., Masek, J., Gascon, F., Dwyer, J., & Choate, M. (2016). A note on the temporary misregistration of Landsat-8 Operational Land Imager (OLI) and Sentinel-2 Multi Spectral Instrument (MSI) imagery. *Remote Sensing of Environment, 186,* 121-122

Strittholt, J., Miles, L., Horning, N., & Fosnight, E. (2007). Sourcebook on remote sensing and biodiversity indicators. In: Secretariat of the Convention on Biological Diversity

Taugourdeau, S., Le Maire, G., Avelino, J., Jones, J.R., Ramirez, L.G., Quesada, M.J., Charbonnier, F., Gómez-Delgado, F., Harmand, J.-M., & Rapidel, B. (2014). Leaf area index as an indicator of ecosystem services and management practices: an application for coffee agroforestry. *Agriculture, Ecosystems & Environment, 192*, 19-37

Thimonier, A., Sedivy, I., & Schleppi, P. (2010). Estimating leaf area index in different types of mature forest stands in Switzerland: a comparison of methods. *European Journal of Forest Research, 129,* 543-562

Urrutia, J. (2010). Validation of the Leaf Area Index product from MODIS-15 for Rice using a Soil-Leaf-Canopy Radiative Transfer Model: A case study of Seville, Spain. In: MSc Thesis, Twente University, Netherland. Retrieved May 8 2013 from www…

USGS (2017). Landsat 7 Landsat Missions. United States Geological Survey.
van den Hurk, B.J., Viterbo, P., & Los, S.O. (2003). Impact of leaf area index seasonality on the annual land surface evaporation in a global circulation model. *Journal of Geophysical Research: Atmospheres, 108*

Verhoef, W. (1985). A scene radiation model based on four-stream radiative transfer theory. In: Nationaal Lucht-en Ruimtevaartlaboratorium

Viña, A., Gitelson, A.A., Nguy-Robertson, A.L., & Peng, Y. (2011a). Comparison of different vegetation indices for the remote assessment of green leaf area index of crops. *Remote Sensing of Environment, 115*, 3468-3478

Viña et al. (2011b). Comparison of different vegetation indices for the remote assessment of green leaf area index of crops. *Remote Sensing of Environment, 115*, 3468-3478

Wang, Q., Zhang, Y., Onojeghuo, A.O., Zhu, X., & Atkinson, P.M. (2017). Enhancing spatio-temporal fusion of modis and landsat data by incorporating 250 m modis data. *IEEE Journal of Selected Topics in Applied Earth Observations and Remote Sensing, 10,* 4116-4123

Weiss, M., & Baret, F. (2016). S2ToolBox Level 2 Products: LAI, FAPAR, FCOVER, Version 1.1. *ESA Contract nr 4000110612/14/I-BG*, 52

Wilhelm et al. (2000). Comparison of three leaf area index meters in a corn canopy. *Crop Science, 40,* 1179-1183

Yang, D ,.Su, H., Yong, Y., & Zhan, J. (2015). MODIS-Landsat Data Fusion for Estimating Vegetation Dynamics–A Case Study for Two Ranches in Southwestern Texas. In, *Proceedings of the 1st International Electronic Conference on Remote Sensing*

Zeng, X., Dickinson, R.E., Walker, A., Shaikh, M., DeFries, R.S., & Qi, J. (2000). Derivation and evaluation of global 1-km fractional vegetation cover data for land modeling. *Journal of Applied Meteorology, 39*, 826-839

Zhu, Z., Wang, S., & Woodcock, C.E. (2015). Improvement and expansion of the Fmask algorithm: Cloud, cloud shadow, and snow detection for Landsats 4–7, 8, and Sentinel 2 images. *Remote Sensing of Environment, 159*, 269-277